Applied Research and Innovation Branch

GEOSYNTHETIC WALL PERFORMANCE: FACING PRESSURE AND DEFORMATION

Peter Hoffman, Research Professor
Jonathan Wu, Professor of Civil Engineering
University of Colorado Denver

Report No. CDOT-2017- 03
February 2017

The contents of this report reflect the views of the authors, who are responsible for the facts and accuracy of the data presented herein. The contents do not necessarily reflect the official views of the Colorado Department of Transportation or the Federal Highway Administration. This report does not constitute a standard, specification, or regulation.

Technical Documentation Page

1. Report No.	2. Government Accession No.	3. Recipient's Catalog No.
CDOT-2017-03		

4. Title and Subtitle	5. Report Date
GRS Wall Performance: Facing Pressure and Deformation	February 2017
	6. Performing Organization Code

7. Author(s)	8. Performing Organization Report No.
Peter Hoffman and Jonathan Wu	CDOT-2017-03

9. Performing Organization Name and Address	10. Work Unit No. (TRAIS)
Reinforced Soil Research Center Department of Civil Engineering University of Colorado Denver CB-113, 1200 Larimer Street, Denver, CO 80217	11. Contract or Grant No. 214.05b

12. Sponsoring Agency Name and Address	13. Type of Report and Period Covered
Colorado Department of Transportation - Research 4201 E. Arkansas Ave. Denver, CO 80222	Final Report
	14. Sponsoring Agency Code

15. Supplementary Notes

Prepared in cooperation with the US Department of Transportation, Federal Highway Administration

16. Abstract

The objective of the study was to validate the performance of blocked-faced Geosynthetic Reinforced Soil (GRS) wall and to validate the Colorado Department of Transportation's (CDOT) decision to waive the positive block connection for closely-spaced reinforcement, defined in report FHWA-HRT-11-026.

Contrary to conventional wisdom, the GRS wall measurements of this study demonstrated that facing pressure decreases as load increases. This counter-intuitive fact is due to the decrease of compaction-induced stress (CIS) with increased load. Therefore, if a GRS wall survives compaction, it survives indefinitely.

Implementation

Pilot specifications for projects selected by the CDOT Bridge Design and Management Branch and allowed by CDOT Regions for trial or demonstration must be developed specifically for each experimental GRS wall construction project. Continued successful application of pilot specifications that waive the use of positive facing connection for closely-spaced reinforcement in GRS design and construction will generate significant support for their acceptance.

17. Keywords	18. Distribution Statement
reinforced soil, geosynthetic, GRS, closely-spaced, facing pressure	This document is available on CDOT's website http://www.coloradodot.info/programs/research/pdfs

19. Security Classif. (of this report)	20. Security Classif. (of this page)	21. No. of Pages	22. Price
Unclassified	Unclassified	75	

CDOT/FHWA RESEARCH STUDY PANEL

Daniel Alzamora – FHWA Resource Center/Colorado Division
Roberto DeDios – CDOT Applied Research and Innovation Branch
Matt Greer – FHWA Colorado Division
Richard Griffin - CDOT Applied Research and Innovation Branch
Jay Hendrickson – CDOT Region 1 Design and Construction
Roman Jauregui – CDOT Region 1 Design and Construction
Aziz Khan – CDOT Applied Research and Innovation Branch
Ilyess Ksouri – CDOT Materials and Geotechnical Branch
Tawedrose Meshesha – CDOT Bridge Design and Management Branch
Ty Ortiz – CDOT Materials and Geotechnical Branch
Larry Quirk – CDOT Region 1 Design and Construction
David Thomas – CDOT Materials and Geotechnical Branch
ShingChun "Trever" Wang – CDOT Bridge Design and Management Branch

EXECUTIVE SUMMARY

The objective of the study was to validate the performance of blocked-faced Geosynthetic Reinforced Soil (GRS) wall and to validate the Colorado Department of Transportation's (CDOT) decision to waive the positive block connection for closely-spaced reinforcement.

Chapter 3 compares estimates and measurements for the instrumented GRS wall on I-70 over Smith Road. For simple access to this report, the reader can proceed directly to Chapter 3. As a research report, the theoretical development of Chapter 2 verifies and validates the analytical approach employed in Chapter 3.

Contrary to conventional wisdom, the GRS wall measurements of this study demonstrated that facing pressure decreases as load increases. This counter-intuitive fact is due to the decrease of compaction-induced stress (CIS) with increased load. Compaction's effect is eventually lost before ultimate capacity, but these measurements reveal that CIS decreases nearly linearly as load increases. Therefore, if a GRS wall survives compaction, it survives indefinitely.

Compaction is a temporary load, but a component of facing pressure is due to long-term dead and live loads. For GRS walls, with their closely spaced reinforcement, this component is shown analytically to be about 12 psf, which is much smaller than 144 psf of average CIS left by a plate compactor. Both analysis and laboratory data show that load-based facing pressure is present in GRS walls, but it is small and hidden by CIS.

The above attribute makes GRS walls appealing. When load exceeds a certain value (q_{ult}) which is the factored ultimate capacity of a vertical reinforced soil wall with a level crest, this GRS attribute is lost. According to both analysis and laboratory data, facing pressure then surges to the Rankine pressure.

While this report addresses friction-connected block facing, it is also applicable to the two-stage facing that has become popular. The two-stage method attaches concrete panels to a wire wall. The method interferes minimally with earth moving operations, and it enables a nicely finished appearance. Soil mechanics indicates that GRS behavior prevents soil plasticity in the core of the soil layer and thereby improves long-term performance. Reinforcement must be closely spaced, or more precisely, the ratio of spacing to aggregate size cannot exceed a threshold value

Finite element analysis, with PLAXIS, was useful in this report. First, it was used to verify hand calculations for simple soil structures. Second, it was used to study geometric changes, for example, reduced deformation due to the geometry of an embankment. The GRS Wall of this study functions in the elastic regime, where finite element analysis is most accurate. The elastic constant for the finite element soil model is taken from the hand calculation in Appendix G.

Finally, a GRS design can be created with the addition of secondary reinforcement or tails. Although secondary reinforcement was not employed on this project, it is discussed in Appendix K.

Implementation Statement

This project validates the analysis of Wu and Payeur (2014) that asserts the adequacy of friction-connected eight-inch blocks when the reinforcement is between every block course. Thus, the requirement for positive facing connection in the design and construction of GRS walls can be waived by CDOT in these situations. To completely implement this finding, responsible staff personnel from CDOT Bridge Design and Management Branch, CDOT Materials and Geotechnical Branch, Regions and CDOT Specifications Unit and technical committees involved in highway design and construction need to collaborate in developing pilot specifications and/or special provisions that do not require positive facing connection for GRS walls.

Pilot specifications for projects selected by the CDOT Bridge Design and Management Branch and allowed by CDOT Regions for trial or demonstration must be developed specifically for each experimental GRS wall construction project. Continued successful application of pilot specifications that waive the use of positive facing connection for closely-spaced reinforcement in GRS design and construction will generate significant support for their acceptance. A proven record of good field performance of constructed GRS walls without positive facing connection will help establish the required project special provisions. The routine and long-term use of these special provisions in future projects with GRS components will eventually lead to the development of the appropriate CDOT standard specifications.

NOMENCLATURE

symbol	definition
D_{max}	largest particle diameter in a homogeneous aggregate
E_S	$100\ K_P\ (p_a\ \sigma_H)^{1/2}$, compressive Young's modulus for a reinforced soil layer
E_R	$T_f/(\varepsilon_R\ S_V)$, tensile Young's modulus for a reinforced soil layer
H	height of reinforced soil structure
K	σ_H / σ_V
K_A	$\sigma_3 / \sigma_1 = \tan^2(45° - \phi/2)$, plastic yield criterion for an aggregate
K_P	$\sigma_1 / \sigma_3 = 1/K_A$, plastic yield criterion for an aggregate
K_o	K at rest, which can be significantly increased by compaction
K_{face}	K at the face, distinguished from K in interior of the soil layer
L_o	optimal lift, associated with optimal compaction induced stress, s_o
M	K/K_A, sometimes called *mobilization* in journals
P	line load (e.g., lb/ft) due to roller compactor
p_a	atmospheric pressure
q	load
q_{ult}	maximum load or capacity achievable without facing
Q_{ult}	$K_P\ T_f/S_V$, maximum load or capacity achievable with incremental facing
s	compaction induced stress (CIS)
s_o	optimal compaction induced stress, associated with optimal lift, L_o
S_V	vertical spacing of reinforcement
T	tension in reinforcement
T_f	tensile strength of reinforcement (ASTM 4595)
T_{max}	tension in reinforcement that reflects AASHTO load factors
W	q_{ult}/Q_{ult}, value of λ associated with elastic-plastic transition of soil layer
γ	weight density of the soil
$\varepsilon_H, \varepsilon_L, \varepsilon_x$	horizontal or lateral strain
$\varepsilon_V, \varepsilon_z$	vertical strain
ε_y	strain in 3rd direction ($\varepsilon_y = \varepsilon_x$ for pier; $\varepsilon_y = 0$ for plane strain)
ε_R	reinforcement strain at rupture (ASTM 4595)
λ	q/Q_{ult} , load factor
ν	Poisson's ratio, approximately 1/3 for common aggregates
$\sigma_H\ ,\ \sigma_L\ ,\ \sigma_x$	horizontal or lateral stress, which has *max*, *min*, and *avg* values
$\sigma_V\ ,\ \sigma_z$	vertical stress
σ_y	stress in 3rd direction ($\sigma_y = \sigma_x$ for pier; plane strain σ_y for wall or abutment)
$\sigma_1\ ,\ \sigma_3$	major and minor principal stresses
ϕ	angle of internal friction of the soil

1. INTRODUCTION

The objective of the study is to validate the performance of blocked-faced GRS wall (I-70 over Smith Road, Aurora, Colorado) and to validate CDOT's decision to waive the positive block connection for closely-spaced reinforcement.

AASHTO (2012) asserts that $T_{max} = \sigma_H S_V$, where σ_H may involve load factors greater than one. Because $\sigma_V/\sigma_H \le K_P$ and $T_{max} \le T_f$, it follows algebraically that the load always satisfies $\sigma_V \le K_P \sigma_H = K_P T_{\max} / S_V \le K_P T_f / S_V$ and that its maximum value, within a vertical reinforced soil wall with a level crest, cannot exceed

$$q_{ult} = K_P \frac{T_f}{S_V} \tag{1}$$

where T_f = tensile strength of reinforcement per unit width, S_V = vertical spacing of reinforcement, and K_P = coefficient of passive lateral earth pressure = $\tan^2(45° + \phi/2)$ for an aggregate (Hoffman and Wu 2015, Hoffman 2015, Hoffman 2016, Elmagre and Hoffman 2016). Appendix A validates Equation (1); however, the reader is cautioned by Mr. Alzamora of FHWA that this equation may not be accepted by some organizations.

In 2011, FHWA published FHWA-HRT-11-026, *Geosynthetic Reinforced Soil Integrated Bridge System Interim Implementation Guide* (Adams et al. 2011). For short, the publication is often called the "GRS-IBS Interim Guide." Paralleling the AASHTO approach, the guide replaces σ_H by the factored load σ_H / W, which reflects increased stress in soil near the reinforcement, and decreases estimated capacity to

$$q_{ult} = WK_P \frac{T_f}{S_V} \tag{2}$$

Henceforth, big Q and small q are used herein for the larger value and smaller value, that is, for Equation (1) and Equation (2), respectively. The difference is the W-factor. Reinforced soil's W-factor is nearly identical to steel's U-factor for shear lag (AISC 2011). Steel, concrete, and all other construction materials exhibit shear lag, that is, σ_H decreases with distance from the beam web or soil reinforcement.

Both Equations (1) and (2) provide accurate estimates of real behavior, but careful interpretation is necessary. The smaller value, Equation (2), represents transition from composite behavior to decoupled behavior, which is associated with bulging, creep, and long-term instability. These phenomena affect facing pressure, the subject of this study.

At the smaller value, the pressure coefficient at the face reaches its maximum. The movement of soil toward the face is a result of an observable "transition" from composite to decoupled behavior.

In summary, Equation (1) and Q_{ult} correspond to capacity with a robust facing. Equation (2) and q_{ult} correspond to unfaced capacity. Wu and Payeur (2014) provide criteria for robust facings in common GRS construction. Assume that the face is vertical and frictionless and that any surcharge is horizontal.

The value of the pressure coefficient at the face can be found by hand calculation. The coefficient is also related to deformation, both elastic and plastic. The latter is simply permanent deformation, which is not recovered if a load is removed.

Section 2 of this report provides analysis. Section 3 applies the analysis to the instrumented GRS wall. Section 4 offers Conclusions and Recommendations.

2. ANALYSIS

2.1 Capacity

2.1.1 Transition

In 1923, von Kármán investigated shear lag in wide-flanged steel beams (Timoshenko 1970). During beam flexure, material at the flange tip is less effective than material near the web. This is depicted in Figure 1. Shear lag is determined by the dimensionless parameter, w/t = ratio of width over thickness for the flange.

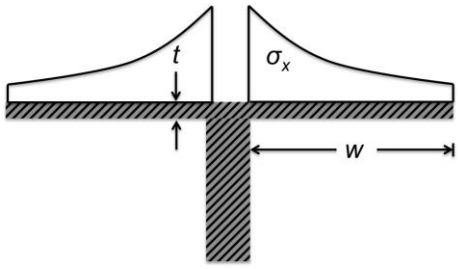

Figure 1. Shear lag in beam flange

In reinforced soil, material at mid-layer is stressed less than material near the reinforcement. This is indicated in Figure 2, borrowing the stress curve from Figure 1.

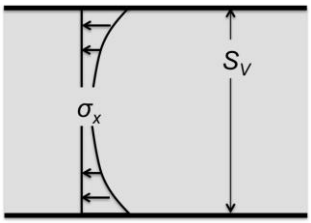

Figure 2. Shear lag in reinforced soil layer

For reinforced soil capacity, Equation (2) can be derived from the Drucker Lower Bound theorem in plasticity. The derivation uses the definition

$$W = \frac{\sigma_x^{\min}}{\sigma_x^{\text{avg}}} \tag{3}$$

where the minimum and average values are taken from the distribution of horizontal stress σ_x in the soil layer, Figure 2.

Transfer of shear through the soil layer is governed by the largest soil particles when the grain size distribution is smooth. D_{max} is the diameter of those particles. As with steel, shear lag of reinforced soil is also determined by a dimensionless parameter, S_V/D_{max}.

Application of Equation (2) requires an estimate of W, which is available as a formula,

$$W = 0.7^{S_V / 6D_{\max}} \tag{4}$$

or as its graph (Wu et al. 2010, Wu and Pham 2013),

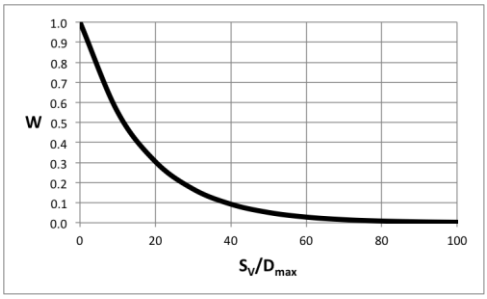

Figure 3. W versus S_V / D_{max}

FHWA conducted a sequence of performance tests (Nicks et al., 2013). This sequence involved pairs, faced and unfaced, of test piers as shown in Figure 4. Equation (1) and Equation (2) correspond to faced capacity and unfaced capacity, respectively. Therefore, W is the ratio of unfaced capacity to faced capacity; that is, $W = q_{ult} / Q_{ult}$.

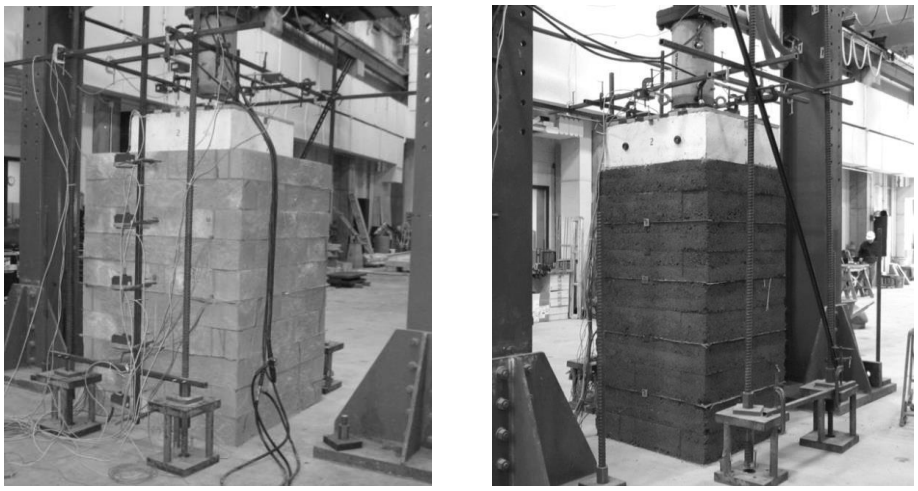

(a) (b)

Figure 4. Pair of FHWA performance tests: (a) faced, (b) unfaced

Capacity ratios for faced/unfaced pairs are listed in Table A.

Table A. Capacities and Ratios for FHWA Test Piers

FHWA Test Pairs	S_V/D_{max}	unfaced capacity (psf)	faced capacity (psf)	ratio W
TF11/TF12	4	23,249	29,030	0.80
TF3/TF2	8	17,491	25,260	0.69
TF13/TF14	12	12,960	23,562	0.55
TF10/TF9	16	10,330	22,310	0.46

As compelling evidence of the facing effect on capacity, Figure 5 compares calculated and measured ratios. The friction angle ϕ has no effect on the ratio.

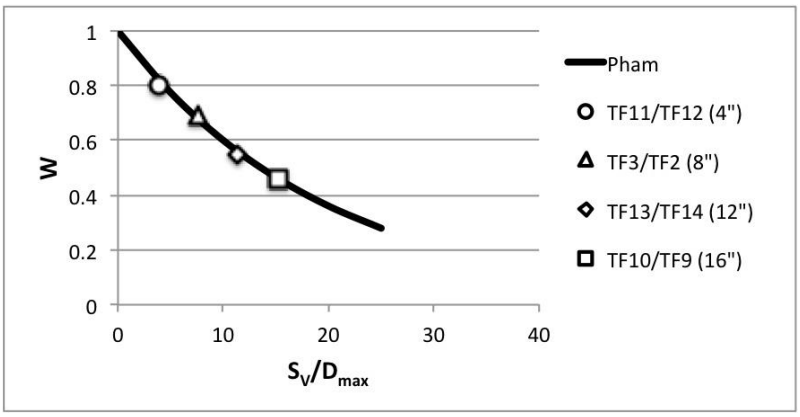

Figure 5. Comparison of FHWA geosynthetic test data with Pham's Equation (4)

For granular soil without cohesion, Equation (2) estimates the load, σ_V, where

$$\frac{\sigma_H^{\min}}{\sigma_V} = K_A = \frac{1}{K_P} \tag{5}$$

That is, the core of the reinforced soil layer fails in accord with Rankine theory. In other words, the core of the reinforced soil layer fails. Soil and reinforcement no longer act as a composite. Transition is this failure of the soil core.

2.1.2 Finite Element Verification of W

In Figure 6, an easy finite element verification of *W* simulates reinforcement by applying shear stress to the top and bottom of a cube of soil.

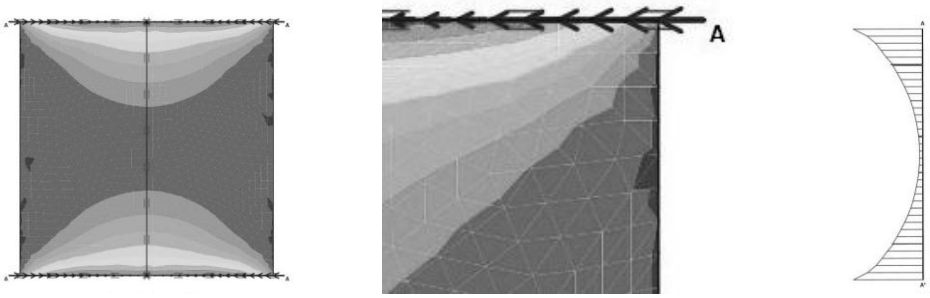

(a) (b) (c)

Figure 6. (a) Non-uniform horizontal stress distribution induced by shear, (b) enlargement of corner where shear stress is greatest, and (c) graph of the resulting horizontal stress distribution, which resembles a parabola.

The horizontal stress distribution in Figure 6 resembles a parabola. And, *W* is the ratio of minimum and average values. This resemblance persists until the transition load, Equation (2).

PLAXIS 8.2 was used for the finite element analysis.

2.1.3 Facing Pressure and Transition

At transition, the core of the soil layer fails, becomes plastic, and moves. If facing is present, the soil moves against it and facing pressure increases. Below the transition load of Equation (2), there is no significant movement. Moreover, there is no significant facing pressure below the transition load. This "soil plug" concept is developed further in Section 2.3.

2.1.4 Validation for Transition

Case studies confirm movement following transition.

CDOT/CU Denver Creep Tests. In 1996, CDOT funded a study of reinforced soil creep with CU Denver. Tests were designed by Wu and conducted by Ketchart (Ketchart and Wu 1996). This 20-year-old CDOT report can now be re-interpreted using shear lag. The sequence involved ten tests, but two are particularly relevant to transition. Test R-1 involved a granular soil and Test C-2 involved clay. Both were loaded to 15 psi (100 kPa). Table B lists parameters of the two tests.

Table B. Parameters of Creep Tests R-1 and C-2

	aggregate (R-1)	**clay (C-2)**
D_{max} / D_{50} *large grain diameter*	1 inch / 0.035 inch (0.0254 m / 0.0009m)	0.2 inch / 0.004 inch (0.005 m / 0.0001 m)
ϕ *soil friction angle*	[1]31°	[2]31°
T_f *tensile strength*	4800 lb/ft (70 kN/m)	4800 lb/ft (70 kN/m)
S_V *vertical spacing*	24 inches (0.6 m)	20 inches (0.5 m)

[1]based on triaxial tests
[2]based on PI = 11 (Terzaghi et al., 1996)

Except for soil grain diameter, D_{max}, the two tests were identical. The transition load, Equation (2), was slightly exceeded by aggregate (R-1) but greatly exceeded by clay (C-2). Both exceeded the transition load, and both experienced creep. However, clay (C-2)

greatly exceeded the transition load, and accordingly, experienced much more creep than aggregate (R-1).

Creep of GW35 (Japan). In 1990, Japan's Public Works Research Institute (PWRI) built a 4.5 m (14 ft) high test wall. It is a geosynthetic wall, called GW35 in the literature (Bathurst et al., 2008). It has a level soil surcharge 0.5 m (19 in) high. Table C lists its parameters.

Table C. Parameters for GW35 (Japan)

ϕ *soil's friction angle*	24°
S_V *vertical spacing*	1.0 m (3.3 ft)
T_f *tensile strength*	59.8 kN/m (4100 lb/ft)
D_{max} *large grain diameter*	1 mm (0.04 in)

At mid-height, self-weight slightly exceeds the transition load. Correspondingly, GW35 exhibits creep that has been monitored for more than a decade.

2.1.5 Capacity Axis

The four cases of creep from Section 2.1.4 can be arranged on a single "capacity axis," Figure 7, relative to the spacing-based or transition capacity and the facing-based capacity. The facing-based and spacing-based capacities are defined by Equations (1) and (2), respectively. GW16 is discussed in Section 2.5.

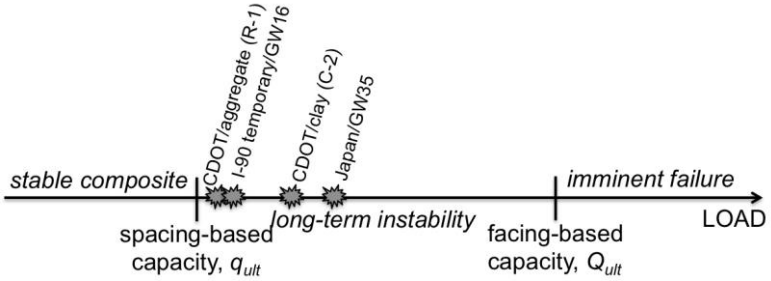

Figure 7. Loads relative to the capacities defined by Equations (1) and (2).

This capacity axis characterizes behavior of reinforced soil structures. Section 2.2 discusses deformation, which presents the opportunity for another axis and for further characterization of reinforced soil behavior.

2.2 Deformation

2.2.1 Deriving K/K_A from Hooke's Law

The American Association of State Highway and Transportation Officials (AASHTO) presents, as in Figure 8, reinforced soil guidance in terms of a normalized pressure coefficient versus soil depth (Allen et al. 2001, Anderson et al. 2012).

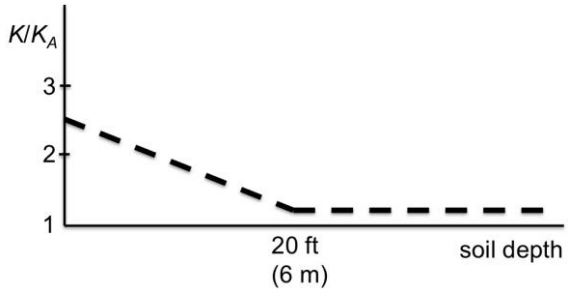

Figure 8. AASHTO Simplified Method for reinforced soil wall of welded wire fabric

The invariant pressure coefficient $K_A = \sigma_3/\sigma_1$ uses principal stresses, and $K = \sigma_H/\sigma_V$ uses stresses in the horizontal and vertical directions. Writing K/K_A is cumbersome, and it is denoted M for mobilized reinforcement strength (Yang, Bathurst, and Zornberg 2010). Then,

$$K = MK_A \tag{6}$$

Because K_A involves principal directions and K involves gravity-aligned directions, M represents a rotation or change of direction.

In the horizontal or x-direction, Hooke's law is

$$e_x = \frac{1}{E}\left(s_x - n\left(s_y + s_z\right)\right) \tag{7}$$

Application of Hooke's law requires that the medium be elastic, isotropic, and homogeneous. These requirements are satisfied for reinforced soil:

- homogeneous - an engineered fill is tumbled before it is placed.
- isotropic - at a microscopic level, soil is extremely directional or non-isotropic. By the statistical law of large numbers, these directional biases cancel at a macroscopic level.
- elastic - aggregates are elastic in compression, and compacted reinforced soil is in compression due to compaction-induced stress (CIS).

From Equation (7), Appendix B derives an equation for $M = K/K_A$ in the case of an FHWA pier and an aggregate.

$$M = \frac{K_p}{2 + 3W \, E_S / E_R} \qquad \text{(FHWA pier)(8)}$$

where the modular ratio involves E_S = Young's modulus for the reinforced soil composite in compression, and E_R = Young's modulus for reinforced soil composite in tension. E_S is determined by soil only, and E_R is determined by reinforcement only.

2.2.2 K/K_A Axis (Quad Chart)

Guided by the AASHTO plot of Figure 8, a useful chart shows K/K_A versus capacity. This is Figure 9.

The right boundary represents the ultimate capacity of Equation (1). For steel, it is the seemingly unfamiliar curve at the upper right of the chart. In fact, this has the most used because the curve represents K_o/K_A and a family of values for $K/K_A > 1$.

The top boundary, $K_P/2$, follows from Equation (8) when the reinforcement is extremely stiff.

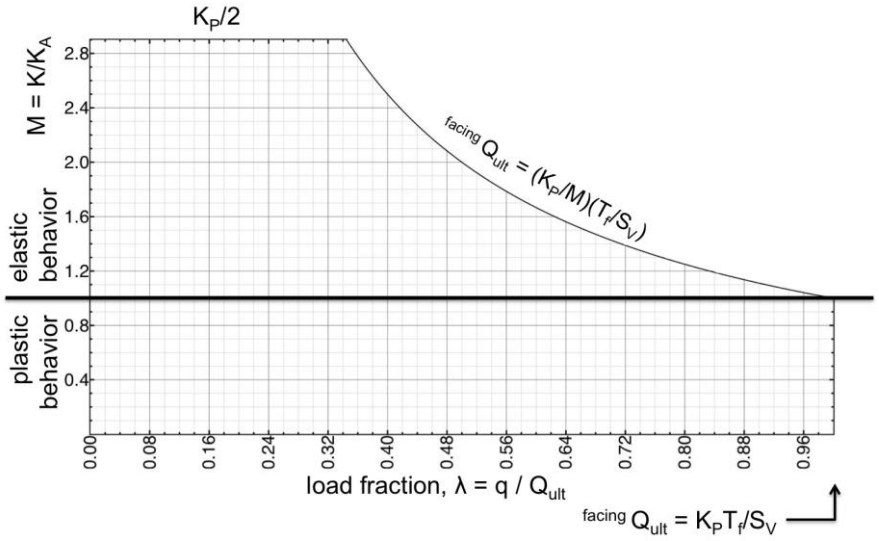

Figure 9. After the AASHTO plots of Figure 8

The bottom axis is the load fraction, λ, relative to the capacity determined by Equation (1). The capacity axis of Figure 7 can be generalized to this chart by drawing a vertical at $\lambda = W$. The vertical line corresponds to Equation (2), and the new chart is Figure 10.

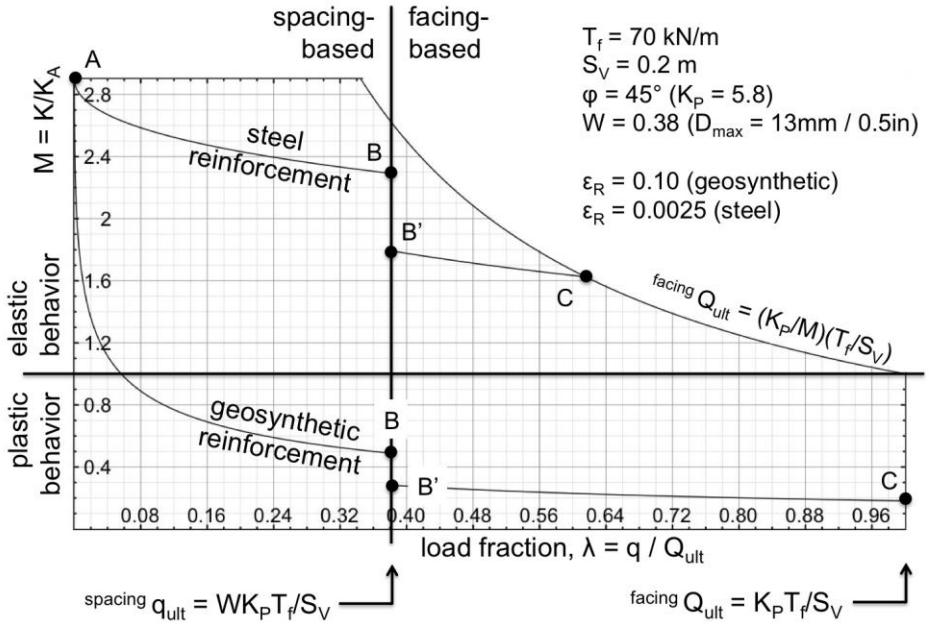

Figure 10. Quad chart for a soil reinforced with geosynthetic or with steel

The chart has four quadrants (a "quad chart") divided by a vertical *W*-line, and the horizontal line at $K/K_A = 1$. The vertical represents transition, and the horizontal represents Rankine ($K = K_A$) solutions.

Appendix D calculates K/K_A at Points A, B, B', and C.

Figure 10 illustrates several key points:

- Steel reinforced soil typically exhibits elastic behavior whereas geosynthetic reinforced soil exhibits plastic behavior.
- Long-term instabilities, such as bulging or creep, occur on the right side of the transition or *W*-line, given by Equation (2).
- Extensibility ε_R plays a critical role in behavior, yet it is seldom well-known or well-specified. Extensibility is reinforcement strain at ultimate strength. It enters Equation (8) as $E_R = T_f/(\varepsilon_R S_V)$ = tensile stiffness of the composite, as shown in the Appendix B.
- Facing pressure is far less with geosynthetics than with steel.

Deformation, both plastic and elastic, is related to K/K_A. Plastic deformation, which is determined from plasticity theory, can be obtained from Figure 11 (Hoffman and Wu 2015). Compaction and batter can control and eliminate plastic deformation.

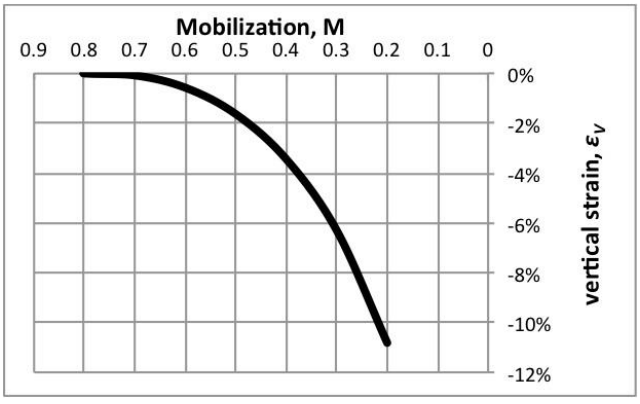

Figure 11. Plastic strain as a function of $M = K/K_A$

Elastic deformation is obtained from E_S, Young's modulus for the soil-reinforcement composite in compression. The value of E_S is found during the calculation of K/K_A; thus, it is highlighted in Appendix D, Table L.

2.2.3 Verification by Finite Element Analysis

Appendix J contains color images of finite element (FE) solutions for the GRS Wall project. Finite element analysis is used to verify aspects of the hand analysis of Sections 2.1 and 2.2. In particular, the distinctive curve of the quad chart shows a relationship between K/K_A and load. By Section 2.4, the relation between load and strain is nearly linear. As a consequence, the relation between K/K_A and strain should resemble the "swoosh curve" relation between K/K_A and load. This is verified by the finite element results shown in Figure 12.

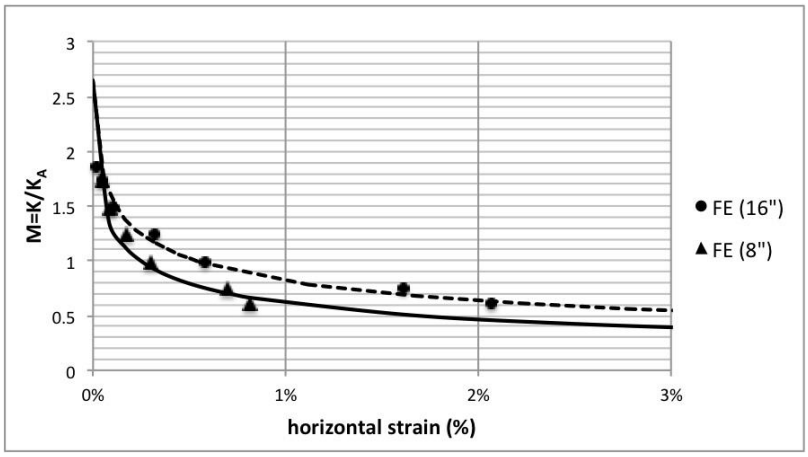

Figure 12. FE verification of quad chart curves in Figure 10: 'K/K_A vs strain' resembles 'K/K_A vs load'.

For Figure 12, the solution process replaced the facing element by a facing pressure. A constant load σ_V was applied, and deformation was computed for several facing pressures, σ_H. So, deformations are obtained for several values of $K = \sigma_H/\sigma_V$. PLAXIS 8.2 was used for the finite element analysis.

In Appendix D, a system of three equations is used to calculate points on the quad chart. This system can be approximated by the single equation, $K/K_A = (K_P/2)/(1+c\sqrt{q})$, where q is the load. For a quad chart, the distinctive curve of a reinforced soil structure is the plot of an equation characterized by c only. As seen in Figure 10, each structure has two curves, which are separated by transition of soil in the core of the layer.

Unfortunately, all finite element software has limitations; for example, there is

- no obvious way to accommodate soil shear lag (grain size) or compaction
- ill-conditioning or stiffness instability when $K/K_A > 1.6$
- instability due to plastic slip and element distortion when $K/K_A < 0.8$

2.2.4 Validation for Quad Chart

Quadrants of the quad chart can be numbered as in trigonometry. That numbering is shown in Figure 13.

Figure 13. Numbering of quadrants

First Quadrant. Because of its failure curve, the first quadrant appears strange, but it is closest to existing methods, typified by use of K_o in Equation (1). For steel reinforced soil, capacity involves division by K where $K > K_A$, and the curve results from that division.

Poorly-behaved steel reinforced soil structures lie in the first quadrant. For validation, consider a steel strip wall constructed at Vicksburg. In the literature, it is known as SS3 (Allen et al., 2001). As indicated in Figure 14, failure of SS3 coincides with the

quadrant's failure curve. $K = K_o$ agrees well in this case. SS3 was built of loose sand, where $K_o = 1 - \sin \phi$ is most applicable (Jaky 1948). More generally, K can be computed as in Appendix D.

Prior to failure, SS3 experienced "significant bulging," which is consistent with having long-term instabilities for loads exceeding Equation (2).

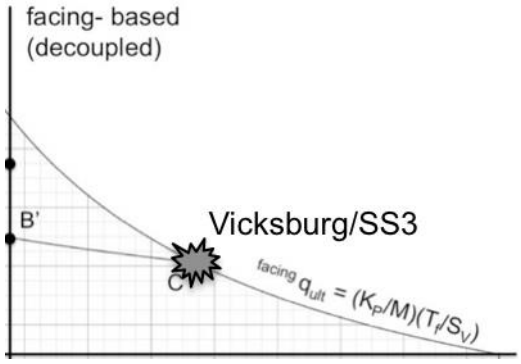

Figure 14. Failure of SS3 lies on the quadrant's failure curve. "Significant bulging" preceded failure.

Second Quadrant. Well-behaved steel reinforced soil structures lie in the second quadrant. As Figure 10 illustrates, their K/K_A curves rise steeply. Consider a welded wire fabric wall, WW1, constructed on I-90 at Rainier Avenue in Seattle (Bathurst, Nernheim, and Allen 2009). Figure 15 compares calculations, measurements, and the design curve of the AASHTO Simplified Method (Anderson et al. 2012, Bathurst et al. 2009). The bends in the curves reflect the transition capacity, Equation (2).

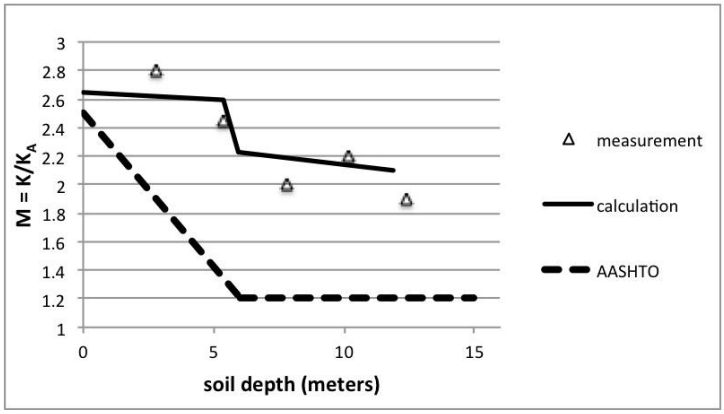

Figure 15. For WW1: comparison of measurements, calculations, and the AASHTO Simplified Method. --- *measurements from Bathurst et al., 2009*

Third Quadrant. Well-behaved geosynthetic reinforced soil structures lie in the third quadrant. Consider four pier tests by Defiance County, OH, and other pioneers (Hoffman and Wu 2015). Values of K/K_A are calculated, converted to deformations, and compared with test data in Figure 16.

Observe that the final test data point departs from the line in each case. This reflects the onset of transition, Equation (2). Transition is also associated with increased facing pressure, Section 2.3.

Transition (near 10000 psf) is clearly demonstrated in Figure 17 for faced and unfaced tests with 16 inch (0.4 m) spacing. These are FHWA Tests TF-9 and TF-10 (Nicks et al. 2013).

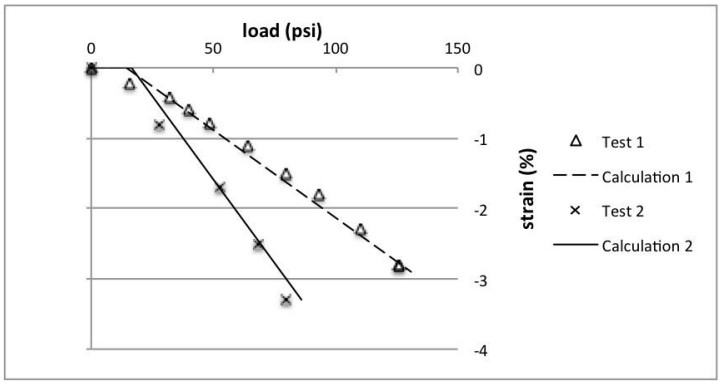

(a)

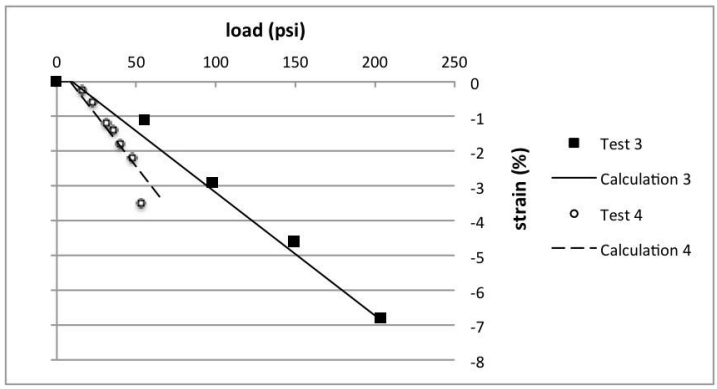

(b)

Figure 16. Calculations and measurements for four pier tests

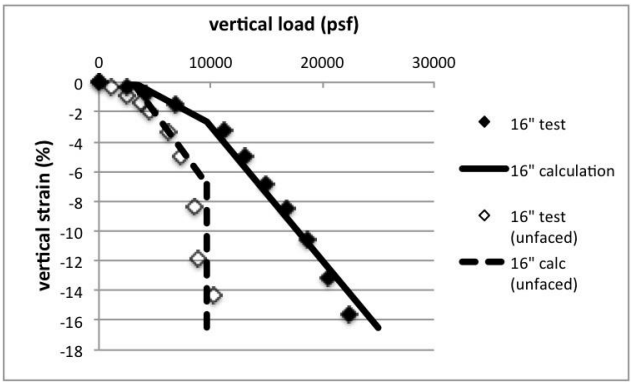

Figure 17. Calculations and measurements for faced and unfaced tests

Fourth Quadrant. The four creep studies of Section 2.1.4 lie in this quadrant. They are displayed in quad chart format as Figure 18.

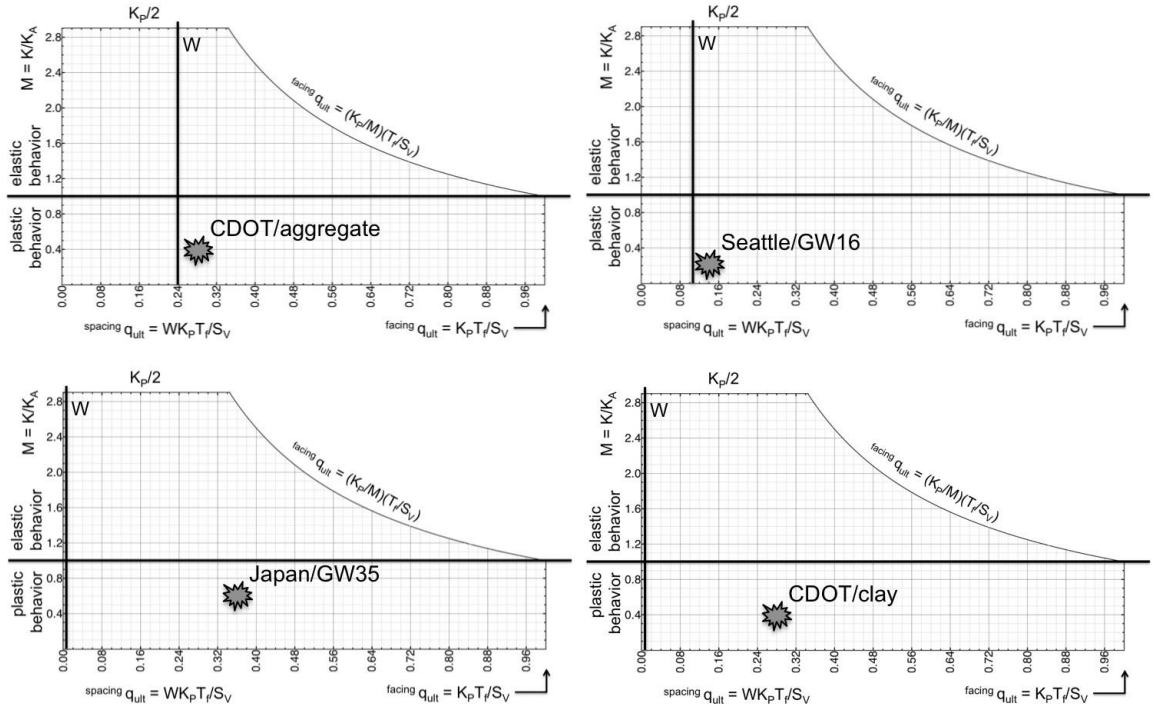

Figure 18. Known instances of creep are right of the *W*-line

2.3 Facing Pressure

2.3.1 Soil Plug and Transition

Facing is material that enables reinforcement tension to develop near the edge of a soil structure. As depicted in Figure 19, the soil itself acts as facing at moderate loads. There is a driving force due to lateral stress in the interior, and there is a resisting force due to friction between the soil plug and the reinforcement. Stability requires adequate friction.

Before transition, strain energy density is greatest in the interior of the soil structure. After transition in a faced structure, strain energy density approaches a uniform maximum value throughout the structure, including the face.

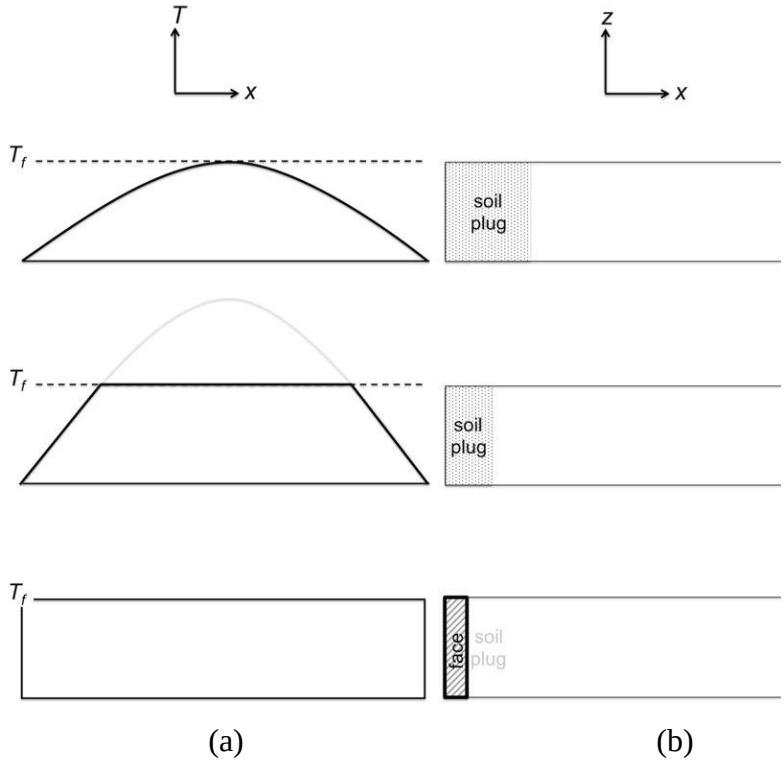

Figure 19. (a) Reinforcement tension *T* cannot exceed T_f as load increases. (b) At small loads, a plug of soil acts as virtual facing. As load increases, plug size decreases. After transition, tension becomes uniform only if there is physical facing.

2.3.2 Coefficient Proportional to Load until Transition

A stable soil plug isolates the face at small loads. Facing pressure is expected to be zero at zero load; however, the pressure coefficient at the face, K_{face} , is also zero due to isolation. The coefficient remains zero until the soil plug decreases with the approach of transition, identified with Equation (2).

At the face, the pressure coefficient K_{face} is inversely proportional to the soil plug size, and that size is inversely proportional to load q; therefore, it is conjectured that K_{face} is directly or linearly proportional to q.

2.3.3 Validation for Facing Pressure

FHWA tests TF-6, TF-9, TF-12, and TF-14 were instrumented for facing pressure (Nicks et al. 2013, Iwamoto et al. 2015). Except for TF-12, each test produced data to loads sufficiently large to show a maximum, indicated in Figure 20.

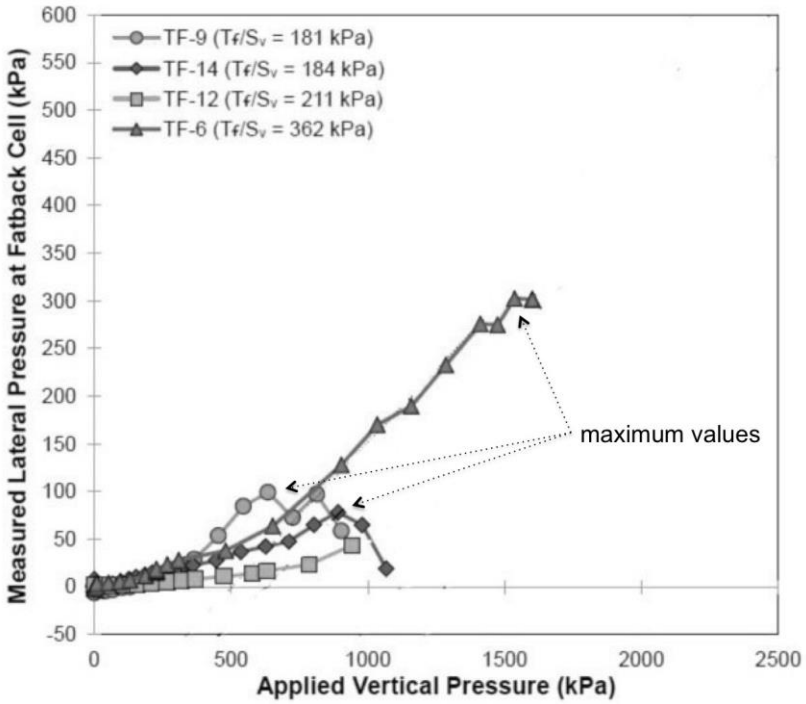

Figure 20. Facing pressures from FHWA tests --- adapted from Iwamoto et al. 2015

In the three tests, maximum facing pressure is observed when the load is approximately 1.25 times the transition load. These locations are calculated as 12560 psf (562 kPa), 15780 psf (707 kPa), and 33180 psf (1790 kPa), for TF-9, TF-14, and TF-6, respectively. Again, the data provide strong evidence that the transition load of Equation (2) is associated with behavioral change in reinforced soil.

While the ratio of facing pressure to load is usually much smaller than K_A, its maximum observed value is approximately K_A. There are two explanations. First, geometry of the tests differ, and the pressure cell cannot be located in the identical position in all tests. Depending upon location, facing pressure fluctuates greatly. Second, K/K_A is usually about 0.3 due to rotation of principal directions, but it approaches one when the face

becomes shear-free (a consequence of Mohr's circle). Facing of an FHWA pier can become shear-free when it separates slightly as the reinforcement ruptures.

The preceding comment applies to geosynthetic reinforcement. For steel reinforcement, the maximum value K of the ratio will satisfy $K/K_A > 1$. Facing pressures in steel reinforced soil are usually much larger than those in geosynthetic reinforced soil.

Based on the observations of Sections 2.3.2 and 2.3.3, maximum facing pressure for geosynthetic reinforced soil has the simple approximation,

$$s_H^{face} = K_{face} q = \left(\frac{q}{1.25 q_{ult}} K_A \right) q = \frac{q^2}{1.25 q_{ult}} K_A \qquad (9)$$

where q = vertical load and $q_{ult} = WK_P T_f / S_V$ = transition load from Equation (2). In summary, it uses the observations that maximum facing pressure coefficient K_{face} is

- linearly proportional to q
- a maximum at approximately 1.25 q_{ult} (if facing is like FHWA performance test)
- K_A when the face is shear-free; otherwise, it is less (for a geosynthetic).

Figure 21 shows validation of Equation (9) in two ways. First, Equation (9) is evaluated and plotted against test data for FHWA Test TF-9.

Second, Equation (9) is inverted. It expresses facing pressure as a function of capacity; therefore, its inverse expresses capacity as a function of facing pressure. This is validated against the GSGC tests at FHWA (Wu et al. 2010). The GSGC tests were shrink-wrapped tests; that is, facing was removed, and using a vacuum-tight membrane, partial atmospheric pressure was applied. Figure 21(b) shows that the calculated capacity agrees with measured capacity.

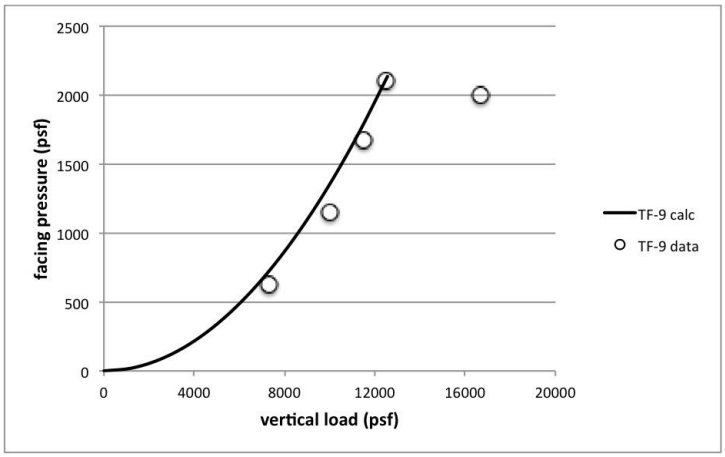

(a)

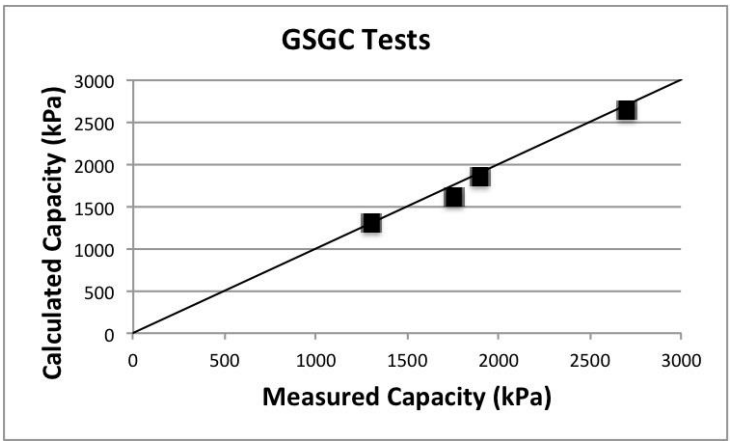

(b)

Figure 21. Validation of (a) Equation (9) against TF-9 data and (b) its inverse against GSGC data

2.4 Facing Deformation

Lateral deformation is calculated and compared with FHWA data from Test TF-7 (Nicks et al., 2013) and from Generic Soil Generic Composite (GSGC) Tests 2 and 4 (Wu et al., 2010). The lateral strain is calculated from deformation measurements at the faces of the test structures.

2.4.1 Elastic and Plastic Strain

For a point and for a small time interval, behavior can be classified as either elastic of plastic. For elastic behavior, the ratio of lateral and vertical strain is $\varepsilon_L / \varepsilon_V = \nu$, Poisson's

ratio. For plastic behavior, $\varepsilon_L / \varepsilon_V = 1$, for dilation-free plane strain. Reinforced soil has little dilation. When averaged over space and time, the ratio lies between these two values; that is, $\nu < (\varepsilon_L / \varepsilon_V)_{avg} < 1$. This report assumes that $\nu \approx 0.33$ for a well-drained granular material.

For lateral strain, the data are sparse, but data from TF-7 and GSGC Test 2 (8 inch spacing) and Test 4 (16 inch spacing) are plotted against the load fraction in Figure 22. The observed range is $0.33 < (\varepsilon_L / \varepsilon_V)_{max} < 0.80$. This observation can be duplicated with GSGC Test 3 (16 inch spacing) and Test 5 (8 inch spacing).

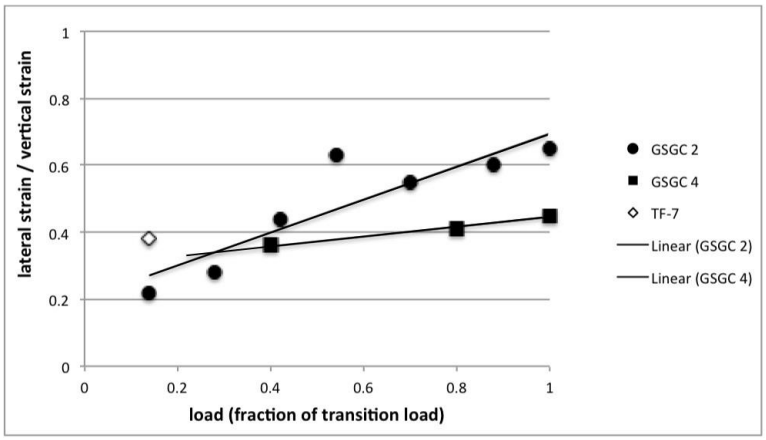

Figure 22. Ratio of lateral and vertical strain as a function of load

Using least squares, lines are fitted to data for GSGC Tests 2 and 4. They intersect near $\nu \approx 0.33$. Data suggest that $\varepsilon_L / \varepsilon_V$ depends on S_V because plastic shear bands are closer when S_V is smaller, as shown by the finite element solution of Figure H-10.

Figure 23 depicts testing of concrete cylinders, where purely elastic zones exist at the loaded surfaces. Reinforced soil structures are similar. The remainder of the structure is a blend of elastic zones separated by plastic shear layers.

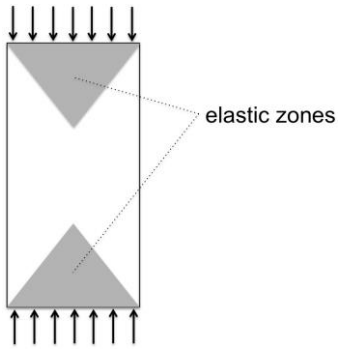

Figure 23. Elastic zones caused by friction. A wall resembles the left or right half of a pier, and lateral stress diminishes toward an unconstrained toe.

For a wall or abutment, B is effectively $0.7H$. Because $H/B \approx 1.4$, GSGC tests are comparable to walls and abutments, and Figure 23 is applicable.

Because Figure 23 is applicable, elastic strain is predominant when the service load is a small fraction of the transition load. For practical applications where the service load is less than 30% of the transition load, $\varepsilon_L / \varepsilon_V = \nu$ is a useful approximation.

2.4.2 Validation for Facing Deformation

By Section 2.4.1, Poisson's ratio relates lateral strain to vertical strain at small service loads. Vertical strain can be elastic or plastic. Tables P and Q of Appendix D calculate K/K_A and E_S at transition load (185 psi) and at service load (25 psi) for pier test TF-7.

First, the plastic approach uses K/K_A (0.26) and Figure 11 to obtain ε_V = 7.9%. This strain, a blend of elastic and plastic strain, is associated with the load-deformation curve of a GRS structure. Both analysis and testing show that this curve is nearly linear up to transition (Adams et al. 2011, Nicks et al. 2013). Scaling linearly to the service load gives

$$\varepsilon_V = \left(\frac{25}{185}\right)(7.9\%) = 1.1\% \tag{10}$$

Second, the elastic approach uses the square pier equation of Table J in Appendix C. Values for K (0.074) and E_S (2.4 ksi) at service load are calculated in Appendix E.

$$\begin{aligned} \varepsilon_V &= \frac{\sigma_V}{E_S}\left(1 - 2\nu K\right) \\ &= \frac{0.025}{2.4}\left(1 - 2(0.33)(0.074)\right) \\ &= 0.99\% \end{aligned} \tag{11}$$

Because the service load (25 psi) is less than 30% of the transition load (185 psi), multiplication by Poisson's ratio gives the lateral strain.

Measured strain for TF-7, shown in Figure 22, compares favorably with calculated strains of Table E.

Table E. Measured and calculated strain for TF-7 at service load

	measured	**calculated**	
		elastic	**plastic**
vertical strain	1.0%	0.99%	1.1%
lateral strain	0.33%	0.33%	0.37%

2.4.2.1 Founders/Meadows Abutment, Colorado

Measured data and computational results were recently published for Founders/Meadows (Zheng et al. 2015). Figure 24 is a one-page hand calculation of its maximum deformation. Figure 25 further validates the method in this report against those published measurements and FLAC computations.

Validation Case: Founders/Meadows Abutment

- T_f = 137,000 lb/ft
- S_V = 16 in
- ϕ = 45°
- D_{max} = 1 in
- ε_R = 10%

uses mid-range value of ϕ; assumes typical values for last two parameters

First, calculate the basic parameters:

- $K_P = \tan^2(45° + \phi/2) = 5.8$
- $W = 0.7^{S_V/6D_{\max}} = 0.39$
- $E_R = \dfrac{T_f}{\varepsilon_R S_V} = 7.2$ ksi
- $q_{ult} = WK_P T_f / S_V = (.39)(5.8)(137000/12)/16 = 1.61 \text{ ksi} = 230{,}000$ psf

Estimate the service load as q = 2% q_{ult} = 4600 psf. *(4400 psf is a typical abutment load.)*

Using λ = 2%, the iteration equations are:

- $\sigma_H = 0.44\lambda MWT_f / S_V = M(.44)(.02)(.39)(137000/12)/16 = 2.5M$ psi
- $E_S = 100K_P\sqrt{p_a\sigma_H}$ psi $= 2.2\sqrt{\sigma_H}$ ksi
- $M = 5.8/(2 + 2.25(WE_S/E_R)) = 5.8/(2 + 0.12E_S)$

Because the service load is small, choose a large initial value for M, e.g., M = 2.

Equation	iteration 1	iteration 2
$\sigma_H = 2.5M$ [psi]	5.0	5.3
$E_S = 2.2\sqrt{\sigma_x}$ [ksi]	4.9	5.1
$M = 5.8/(2 + 0.12E_S)$	2.2	2.2
(M_{init} = 2.0) $M_{average}$:	2.1	2.2

Estimated strains are $\varepsilon_V = (q/E_S)\left(1 - \nu K - \nu^2(1+K)\right) = 0.0045$ and $\varepsilon_H = \nu\varepsilon_V = 0.0015$, where q = 4600 psf = 0.032 ksi, E_S = 5.1 ksi, ν = 0.33, and $K = MK_A$ = 0.38. Based on 20 foot height, the estimated lateral deformation is (0.0015)(20) = 0.03 ft = 0.36 in (9 mm).

Figure 24. The one-page hand calculation for Founders/Meadows.

Figure 25 compares the result with measured data and a FLAC computation.

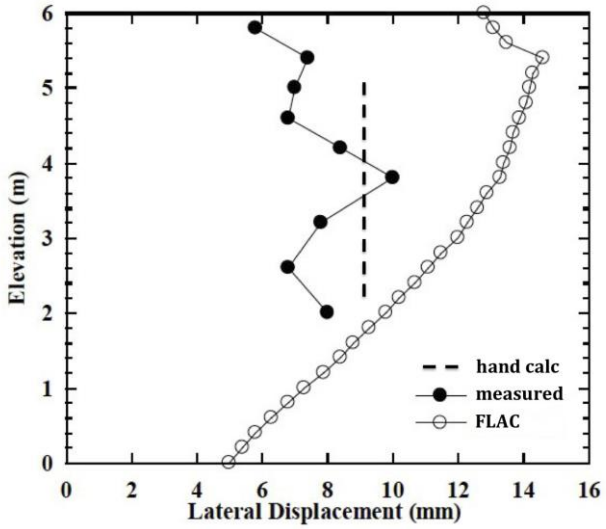

Figure 25. Founders/Meadows. The method of this report (hand calculation) is compared with measured data and FLAC results. -- *after Zheng et al. 2015*

2.5 Reinforcement Strain

Internal deformation is calculated and compared with strain data from a temporary wall on I-90 at Rainier Avenue in Seattle. Used during a year of construction, the geosynthetic wall is identified in the literature as GW16 (Allen and Bathurst 2003).

2.5.1 Calculation of Reinforcement Strain

From Equation (B.3) in Appendix B, Young's modulus in tension of a reinforced soil structure is

$$E_R \circ \frac{T}{e_R S_V} \tag{12}$$

where S_V = vertical spacing, T = reinforcement tension per unit width, and ε_R = reinforcement strain at that tension. By static equilibrium, T/S_V is average horizontal

stress, σ_H. And, $\sigma_H = K\,\sigma_V$ where $K = MK_A$ is calculated in accord with Appendix D. Combining these equations gives the average estimated strain,

$$\epsilon_R^{avg} = \frac{MK_A s_V}{E_R} \tag{13}$$

2.5.2 Validation for Reinforcement Strain

Equation (13) is compared with strain data from GW16 (Allen and Bathurst 2003). This was an instrumented, temporary wall. It was erected during construction and removed one year later.

GW16 had four sections, and the section immediately below mid-height is analyzed and plotted in Figure 26. As estimated by Equation (2), the transition load for GW16 is 2920 psf (140 kPa), but the actual load at mid-height is 4490 psf (215 kPa). But, as estimated by Equation (1), this wall has an ultimate load that is 29200 psf (1400 kPa) or ten times greater. According to these estimates, GW16 was creeping, but its time to failure was longer than its temporary duty of one year.

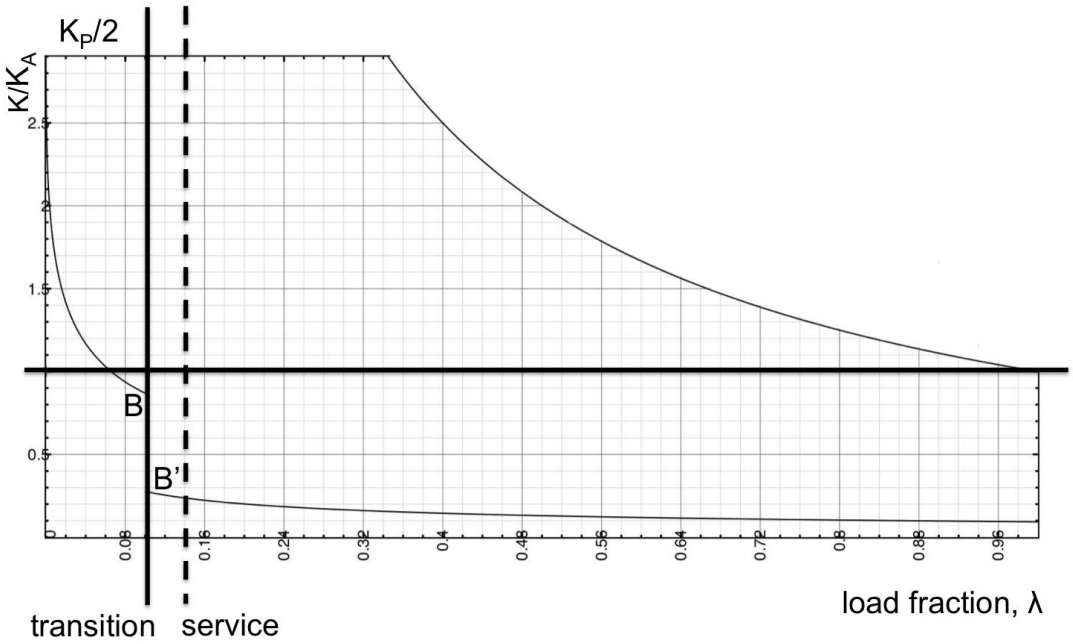

Figure 26. GW16 functioned near its transition load

Reinforcement strength is T_f = 6300 lb/ft (92 kN/m) and spacing is S_V = 15 in (0.38 m). A nominal extensibility of ε_R = 12% is assumed. By Equation (12), E_R = 292 psi (2.0 MPa). At Point B' of Figure 26, $M = K/K_A$ = 0.23, and Equation (13) yields

$$\varepsilon_R^{avg} = \frac{MK_A s_V}{E_R} = \frac{(0.23)(0.17)s_V}{292 \text{ psi}} = \frac{s_V}{7.5 \text{ ksi}} \tag{14}$$

The service load is σ_H = 2920 psf = 0.020 ksi, then ε_R = 0.02/7.5 = 0.3% on average. Because the distribution resembles a parabola, where the average is 2/3 of the maximum, the strain ranges from 0% at the edge to a peak of 0.3/(2/3) = 0.45%. This agrees with the strain measurements of Figure 27.

GW16 was a temporary wall used during construction, but it demonstrated the ill effects of a design that lies on the transition point. Deformation during loading was significant as the structure transitioned from B to B' in Figure 26. Creep was observed throughout the year of the wall's existence.

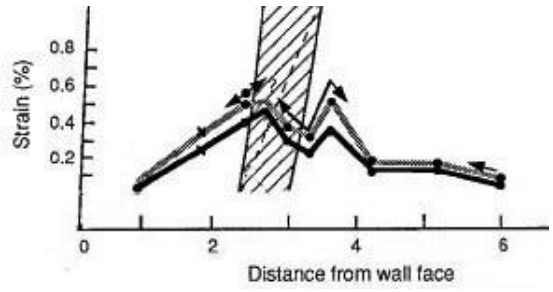

Figure 27. Strain measured in GW16 at mid-height. Strain increased with time. The shear band is shaded. *--- adapted from Allen and Bathurst 2003*

3. APPLICATION TO GRS WALL PROJECT

3.1 Configuration

Figure 28 is a photo of the instrumented GRS Wall on I-70 over Smith Road near Denver. Union Pacific Railroad tracks are in the foreground. Three junction boxes and a solar array are visible on the wall. The right and left boxes are instrumentation junctions for Line 4 and Line 5, respectively.

Figure 28. Photo of instrumented GRS Wall on I-70 over Smith Road

Figure 29 is a drawing for a section of the GRS Wall. It indicates that each instrumentation line supports four elevations with strain gauges on the reinforcement. Each elevation also has horizontal and vertical pressure cells.

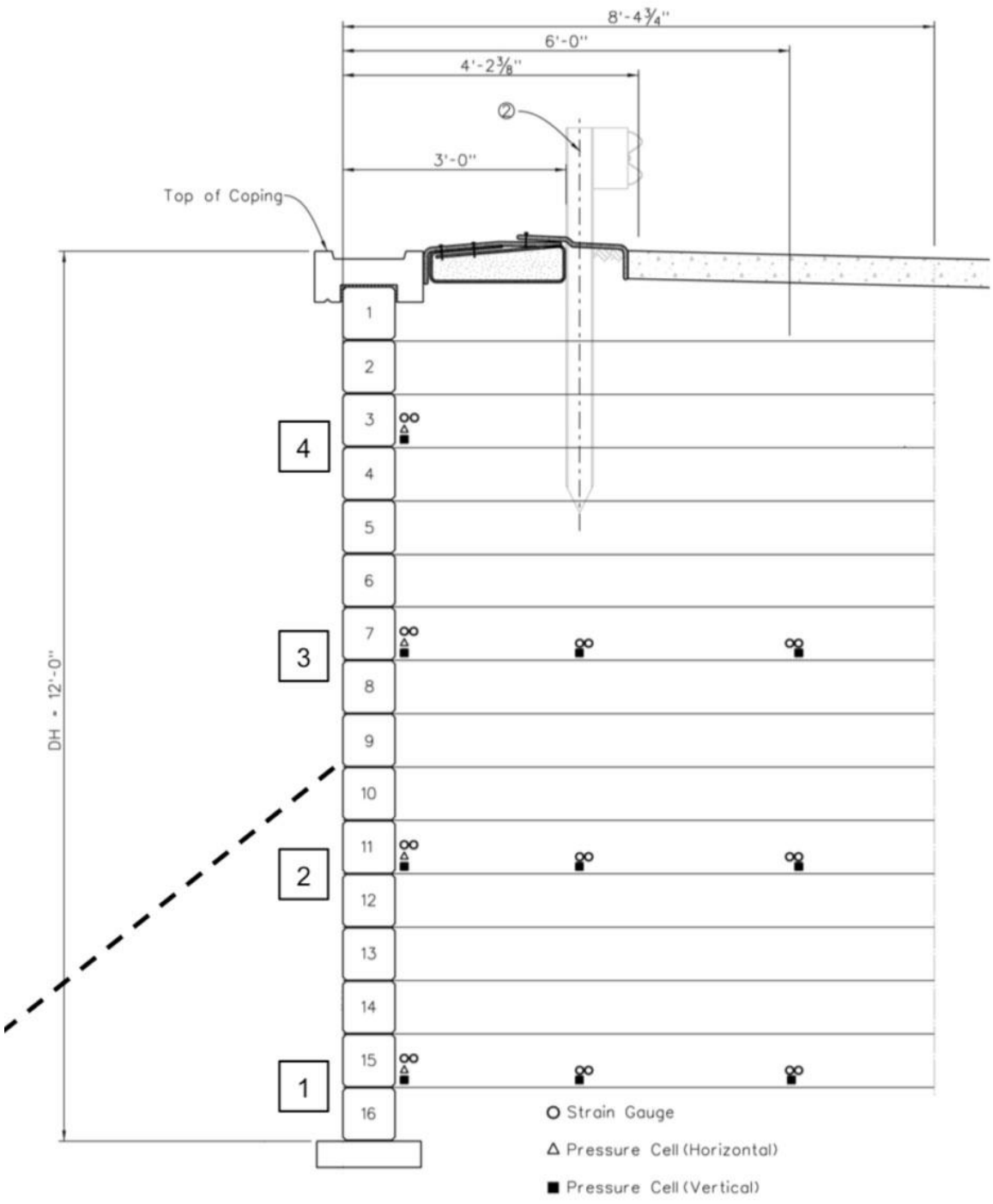

Figure 29. GRS Wall with cells measuring horizontal pressure (Δ) on the facing blocks.

The drawing shows that the wall is nominally 12 feet high. Because the facing courses must step up the approach to the bridge, actual height varies and is usually less. Appendix I provides the configuration at instrumentation Line 4. Nevertheless, the 12 foot value approximates the total load due to soil self-weight, pavement, and lane load.

Table F lists the parameters of the GRS Wall.

Table F. Parameters for the instrumented GRS Wall

H *height*	12 ft (3.7 m)
D_{max} *large grain diameter*	0.4 in (10 mm)
ϕ *soil friction angle*	43°
γ *soil weight density*	142 lb/ft^3 (22.3 kN/m^3)
T_f *tensile strength*	4800 lb/ft (70 kN/m)
ε_R *extensibility*	18%
S_V *vertical spacing*	8 in (0.2 m)

3.2 Estimates

Facing pressure, lateral deformation, and reinforcement strain are estimated. For this purpose, Table G lists approximate loads. Service load includes dead load and self-weight 0.4*H* above the base, which assumes the wall's toe is free to move during loading so that lateral stress diminishes there.

Table G. Approximate loads for instrumented GRS Wall

transition load, q_{ult}	11400 psf (550 kPa)
service load, q	960 psf (53 kPa)

Appendix G calculates a few points for approximation of the GRS Wall's quad chart. At service load, the GRS Wall functions in the upper left (elastic) quadrant of Figure 30.

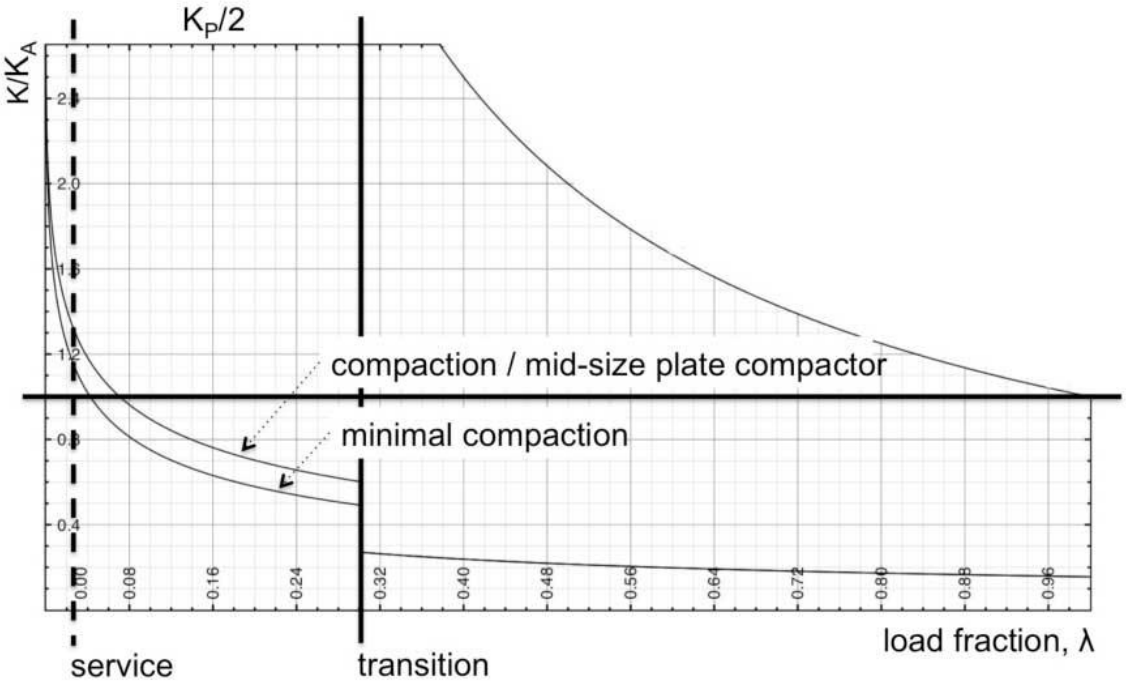

Figure 30. Depending upon compaction, $0.49 < K/K_A < 0.61$ at transition load

3.2.1 Lateral Stress (Facing Pressure)

By Equation (9), facing pressure at service load is

$$s_H^{face} = \frac{q^2}{1.25 q_{ult}} K_A = \frac{(960)^2}{1.25(11400)}(0.19) = 12 \text{ psf } (0.6 \text{ kPa}) \qquad (15)$$

The service load point (960, 12) is indicated by a triangle in Figure 31.

Complicating measurement, the plate compactor introduces compaction-induced stress (CIS) up to 288 psf (14 kPa). This follows from Broms' theory in Appendix H. Average CIS is probably around 144 psf (7 kPa) and decreases with load.

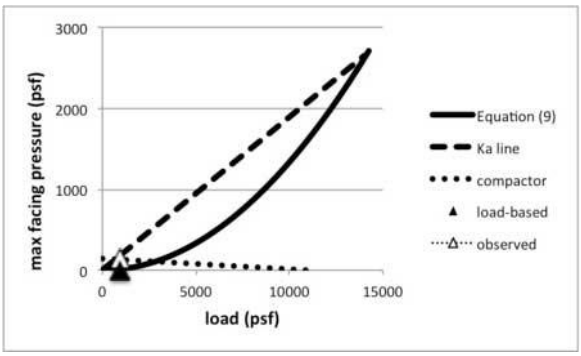

(a)

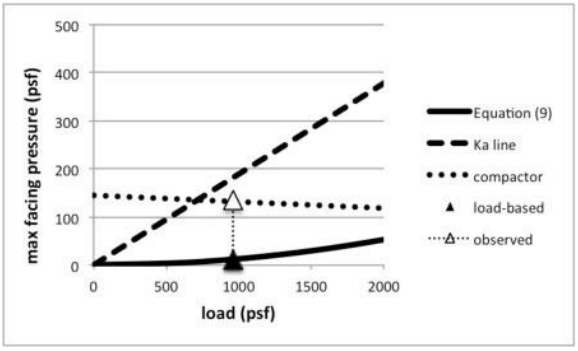

(b)

Figure 31. Maximum lateral stress at the face. In the enlarged view (b), the dotted line is average compactor induced stress (1 psi = 144 psf), which decreases with load.

3.2.2 Lateral Deformation (Facing Deformation)

In Appendix G, Table X precisely calculates E_S = 1.5 ksi and K/K_A = 0.96 (or K = 0.18) at service load with minimal compaction. The plane strain equation of Table J gives vertical strain as

$$\begin{aligned} \varepsilon_V &= \frac{\sigma_V}{E_S}\left(1 - \nu K - \nu^2(K+1)\right) \\ &= \frac{0.0067 \text{ ksi}}{1.5 \text{ ksi}}\left(1 - (0.33)(0.18) - (0.33)^2(0.18+1)\right) \\ &= 0.0036 = 0.36\% \end{aligned} \tag{16}$$

In accord with Figure 22 at service load, multiplication by Poisson's ratio yields the estimated lateral strain, (0.33)(0.36%) = 0.12%.

Table H. Estimated strain near face of unconstrained wall

vertical strain	0.36%
lateral strain	0.12%

For H = 12 feet, the maximum lateral deformation of (0.0012)(12) = 0.014 ft = 0.17 in (4.3 mm) occurs near the middle of the wall as shown in Figure 32. This value is confirmed by finite element analysis with PLAXIS 8.2.

Finite element analysis yields unusually good results because Quadrant Two is elastic. The soil's elastic modulus for finite element analysis is taken from the hand calculation of E_S in Appendix G.

The embankment partially constrains the wall. Finite element analysis shows that the embankment reduces lateral deformation about 20% to 0.14 in (3.5 mm). In Appendix J, Figure I-1 shows the color detail of the finite element solution.

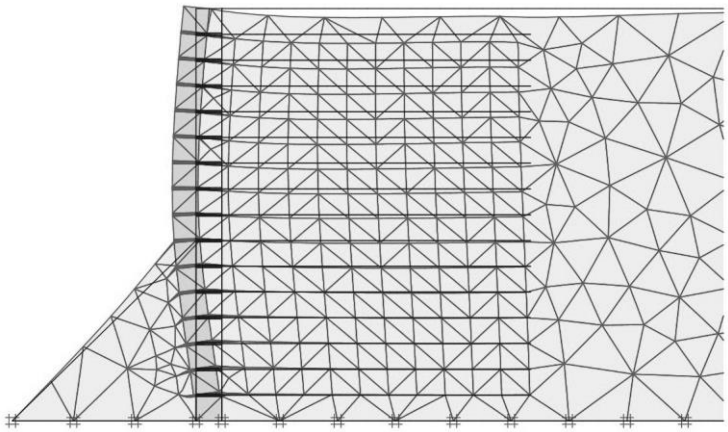

Figure 32. Finite element computation shows deformation (x 50) of the GRS Wall

3.2.3 Reinforcement Strain

Although intended for reinforcement strain, Equation (13) of Section 2.5 provides an alternate calculation concerning lateral deformation. It is based on stiffness of the reinforcement, not the soil. Due to shear lag in GRS, average soil strain is less than reinforcement strain.

At small service loads, the values of $M = K/K_A$ are hugely affected by compaction. In Figure 30, $1.15 < K/K_A$. The minimum value, $K/K_A = 1.15$, is used here to estimate strain. By Equation (12), the Young's modulus of the composite in tension, E_R, is 278 psi. Equation (13) gives average strain in the reinforcement as

$$\varepsilon_R^{avg} = \frac{MK_A\sigma_V}{E_R} = \frac{(1.15)(0.19)(6.7\text{ psi})}{278\text{ psi}} = 0.0053 = 0.53\% \qquad (17)$$

The average strain is associated with a distribution that resembles a parabola; therefore, average values are divided by 2/3 to obtain peak values. Estimated peak reinforcement strain for the as-designed wall is $\varepsilon_R \approx 0.8\%$.

Finite element analysis indicates that lateral deformation is 20% less due to the embankment. Therefore, estimated peak reinforcement strain for the wall is $\varepsilon_R \approx 0.6\%$, which is 6000 microstrain.

3.2.4 Summary of Estimates

Table I summarizes estimates for the GRS Wall.

Table I. Estimates for the instrumented GRS Wall

facing pressure:		
load-dependent	12 psf	(0.6 kPa)
+ compactor (avg CIS)	144 psf	(6.9 kPa)
max lateral deformation	0.14 in	(3.5mm)
max reinforcement strain	0.6%	

3.3 Measurements

Data were provided by the instrumentation contractor, Shannon and Wilson, Inc (Goode and Vessely 2016).

3.3.1 Lateral Stress (Facing Pressure)

In the plots of Figures 33 and 34, lateral stress is measured by the horizontal pressure cells at the face. Vertical pressure is the average of the three measurements at each elevation. Manual logging of data was followed by automated hourly logging in November 2015 when the plots exhibit diurnal variation.

The eight measurements of Figures 33 and 34 resemble the estimated plot of Figure 31, where CIS of approximately 144 psf decreases as load increases. Facing pressure of 12 psf is expected, but this is obscured by the CIS.

Contrary to conventional wisdom, horizontal stress (facing pressure) decreases as vertical pressure (load) increases. This attribute makes GRS walls appealing. When load exceeds q_{ult}, this GRS attribute is lost, and facing pressure becomes Rankine pressure

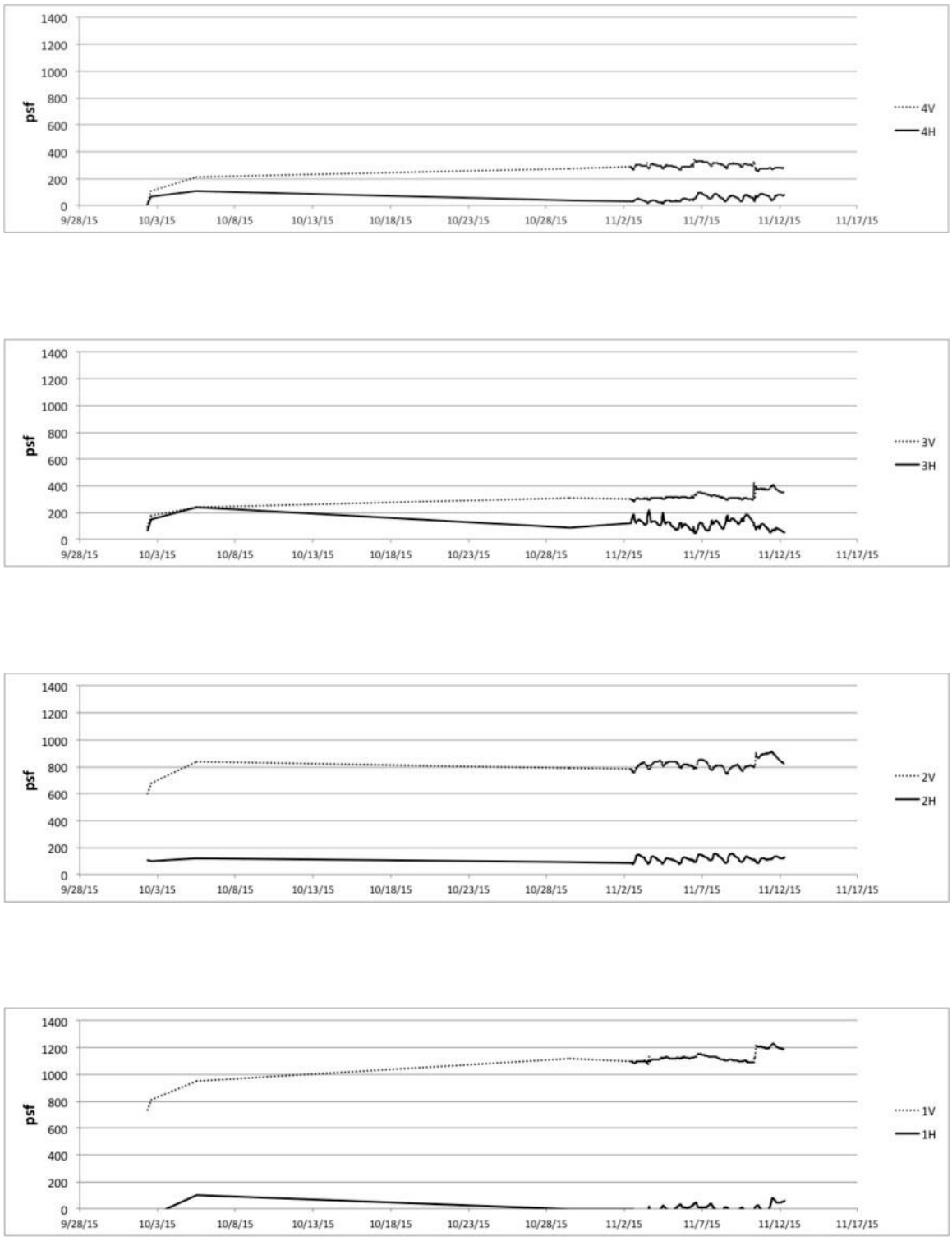

Figure 33. Line 4: vertical (V) and horizontal (H) stresses at the four elevations

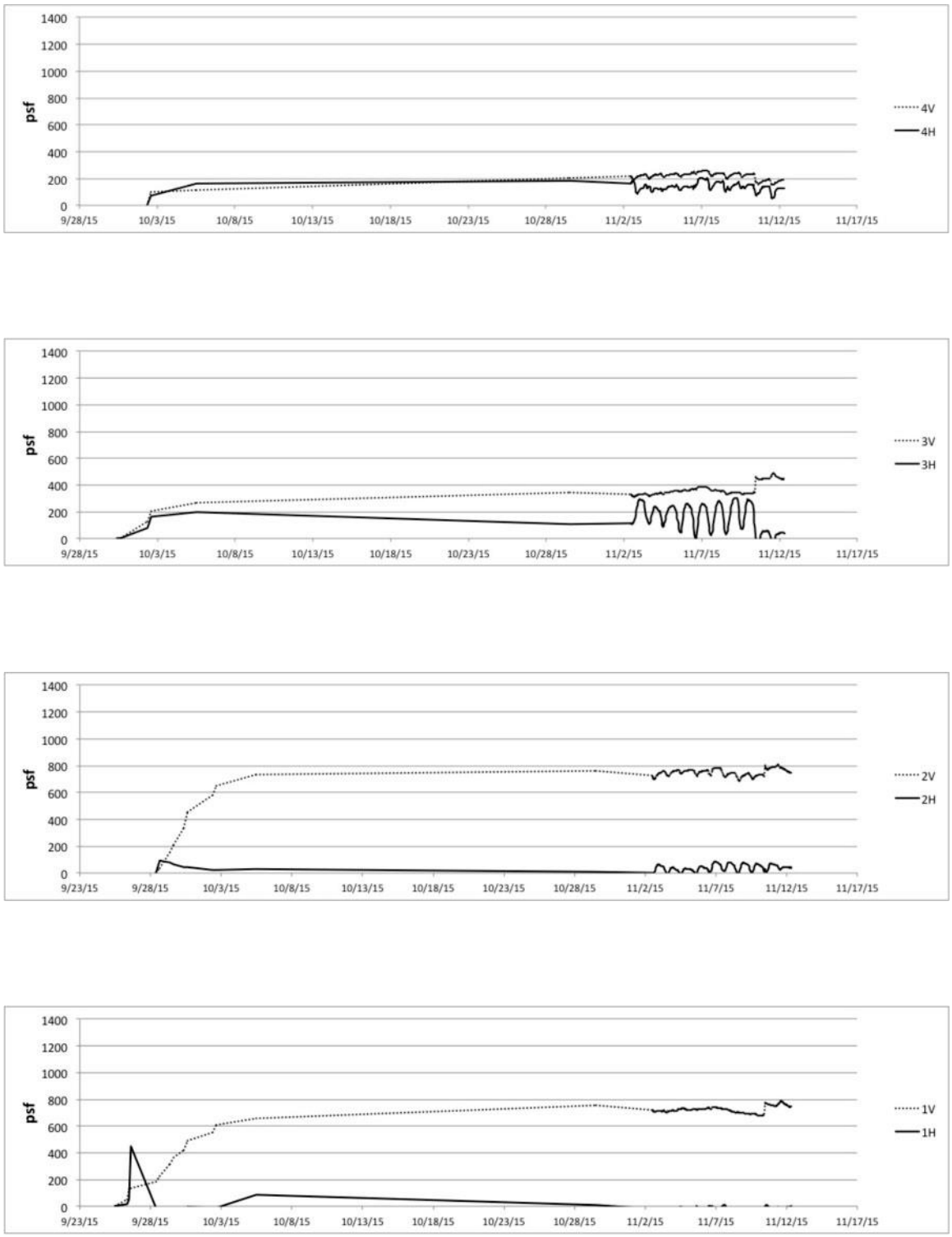

Figure 34. Line 5: vertical (V) and horizontal (H) stresses at the four elevations

3.3.2 Reinforcement Strain

Strain gauges are attached to the reinforcement three and six feet from the face, and also, at the block. Figure 35 demonstrates that strain patterns are similar between Line 4 and Line 5. Strain is greatest near the intersection of the embankment and the facing blocks, agreeing with the finite element analysis of Figure I-2 in Appendix J. Due to shear lag, reinforcement strain exceeds average strain in the soil.

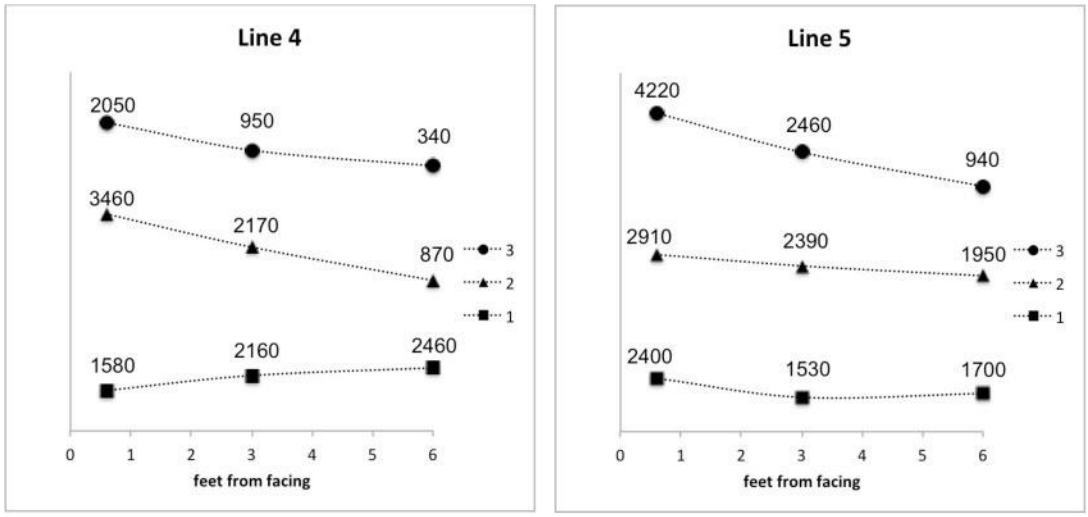

Figure 35. Reinforcement microstrain

Because the GRS Wall functions in Quadrant Two, there is no evidence of plastic behavior or slip lines. Behavior is nicely elastic. Every GRS wall functions in Quadrant Two when its service load is a sufficiently small fraction of the GRS capacity q_{ult}.

The calculation of Section 3.2.3 predicts a maximum microstrain of 6000 (0.6%). The maximum in Figure 35 is only 4220, but pavement and live load are absent at time of measurement. In their absence, load and strain are reduced approximately 300 psf or 30%. The adjusted estimate, (70%)(6000) = 4200, is equal to the measured microstrain.

3.3.3 Summary of Measurements

Data were provided by the instrumentation contractor, Shannon and Wilson, Inc (Goode and Vessely 2016).

Adjusted for absence of pavement and lane load, the estimated maximum reinforcement strain matches the measurement of 4200 microstrain.

Facing pressure (approximately 144 psf) at the GRS Wall is due to compaction, but it diminishes as load increases. If a GRS wall ($q < q_{ult}$) survives compaction, it will survive indefinitely. Appendix K discusses secondary reinforcement (tails) that can convert a design into a GRS design.

It was known that CIS disappears before $q = q_{ult}$, but surprisingly, the measurement data show that CIS appears to decrease linearly as load increases!

From a GRS perspective, no significant variations were recorded in the data during the first six months. The toe of the wall was covered with soil after construction, and being immobilized, it no longer behaves as reinforced soil. The record shows a temporary increase in horizontal stress that coincides with a temporary increase in vertical stress; that is, pressure at the constrained toe behaved as ordinary soil, not reinforced soil.

4. CONCLUSIONS AND RECOMMENDATIONS

Measurements are consistent with the analysis. Facing pressure in GRS walls is due almost entirely to compaction-induced stress (CIS). Because CIS decreases as load increases, a GRS wall that survives compaction will survive indefinitely.

A GRS wall satisfies the relation $q < q_{ult}$, and it exhibits spacing-based behavior. If the load is increased so that $q > q_{ult}$, then the wall transitions to facing-based behavior. Therefore, any wall is a GRS wall for a sufficiently small load. Its facing pressure is due to compaction, and it decreases as load is increased to about $q = q_{ult}$. Instead of decreasing further with additional load, facing pressure suddenly surges toward Rankine pressure ($K_A\ q$). The facing and its connections are stressed by Rankine pressure; nevertheless, a friction-connected block wall will remain stable if the criteria of Wu and Payeur (2014) are satisfied. The criteria are usually satisfied if reinforcement is friction-connected at every block course. Such a GRS wall can be loaded far beyond transition, and this has been shown by FHWA performance tests.

One can also go the other way. For a specific service load, a design can be converted into a GRS design by the introduction of secondary reinforcement (tails). Appendix K analyzes secondary reinforcement.

APPENDIX

A. Validation of Equation (1)

FHWA test data from faced GRS piers (Nicks et al. 2013) demonstrate the accuracy of Equation (1).

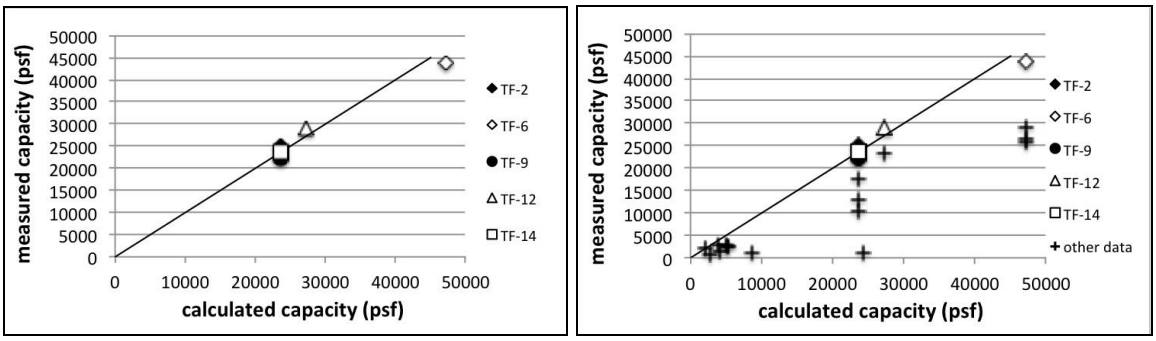

(a) (b)

Figure A-1. In the faced tests of figure (a), data from FHWA's TF-series demonstrate the accuracy of Equation (1). Validating the inequality's bound, figure (b) includes all tests from the TF-series as well as from other publicized failure testing, both steel and geosynthetic. No data lie above the line.

Figure (b) validates the inequality when other data are included, i.e., unfaced GRS tests in the TF-series (Nicks et al. 2013), Vicksburg data for steel reinforced soil (Al-Hussaini and Perry 1978), and other failure data (Allen and Bathurst 2003, Bathurst et al 2008, Wu et al 2006).

Equation (1) has appeared in other publications (e.g., Hoffman and Wu 2015, Hoffman 2015, Hoffman 2016, Elmagre and Hoffman 2016).

Prior to publication of this report, the soil friction angle ϕ used for Figure A-1(a) was discussed among FHWA, CDOT, and the authors. The authors' position:

- FHWA-HRT-13-066 reports that ϕ = 54 degrees is the friction angle of both the well-graded aggregate of the Turner Fairbank (TF) tests, used in Figure A-1(a),

and the 1/2 inch open-graded aggregate of the Defiance County (DC) tests.

- FHWA-HRT-13-068 is a companion report that explains the new direct shear technique used to measure friction angles.

- FHWA-HRT-11-026 reports that, under the old technique, ϕ = 48 degrees for the the 1/2 inch open-graded aggregate of the DC tests. This six degree difference suggests that, under the old technique, ϕ = 48 degrees for the TF tests, too.

- FHWA-HRT-10-077 (page 66) reports triaxial data, shown in Figure A-2, for the soil used in the Turner Fairbank (TF) tests. The tangent angle to the envelope varies with confining pressure. For TF tests, $\sigma_3 = T_f / S_V$ = 30 psi, and triaxial data confirm that the angle is approximately ϕ = 48 degrees.

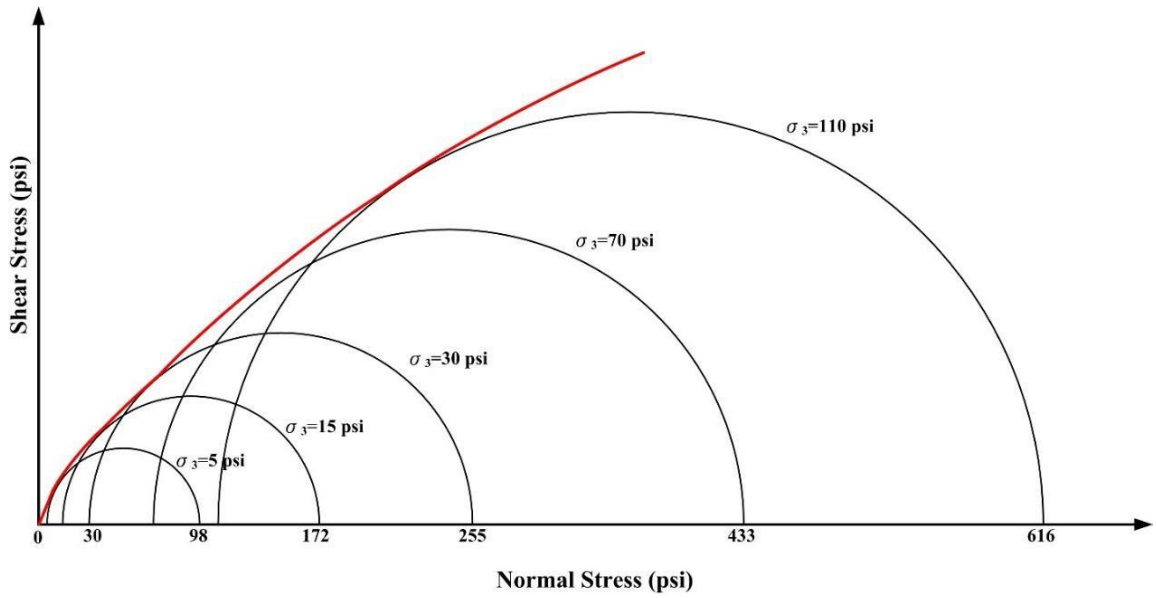

Figure A-2. Triaxial data for the TF-series tests. The tangent angle to the envelope varies with confining pressure. For TF tests, the angle is approximately ϕ = 48 degrees.

B. Derivation of K/K_A from Hooke's Law

This Appendix introduces the concept of mobilization (or K/K_A) in order to determine capacity and deformation of reinforced soil. Reinforced soil structures exhibit elastic behavior if the mobilization $M = K/K_A \geq 1$. Otherwise, behavior is plastic. The equation for mobilization is derived from Hooke's law. The derivation by Hoffman and Wu (2015) involves four assumptions in subsections B.1 through B.4 that follow.

B.1 Assumption: Horizontal Equilibrium

The tensile force is equal to the compressive force, or $T = C$ as in reinforced concrete. The compressive force is

$$C = \sigma_x^{\text{avg}} S_V \tag{B.1}$$

where S_V = vertical spacing of the reinforcement and σ_x^{avg} = average horizontal stress in the soil. Hooke's law involves Young's modulus, and the tensile modulus E_R of a layer of reinforced soil composite is required. In the absence of cohesion, the tension T is borne entirely by the reinforcement,

$$T = \varepsilon_R E_R S_V \tag{B.2}$$

where ε_R = strain in the reinforcement at tension T. This implicitly defines E_R so that

$$E_R = \frac{T}{\varepsilon_R S_V} \tag{B.3}$$

Because $T = C$, conclude that

$$\varepsilon_R E_R = \sigma_x^{\text{avg}} \tag{B.4}$$

B.2 Assumption: Strain Compatibility

In the absence of pullout, strain in the reinforcement is equal to strain in the adjacent soil; that is,

$$\varepsilon_R = \varepsilon_x^{\max} \tag{B.5}$$

B.3 Assumption: Shear Lag

The distribution of horizontal stress or strain may not be uniform. Let W denote the ratio of the average horizontal strain to the maximum strain; that is,

$$W = \frac{\varepsilon_x^{\text{avg}}}{\varepsilon_x^{\max}} \tag{B.6}$$

Combining Equations (B.4) - (B.6) gives

$$\varepsilon_x^{\text{avg}} = W\varepsilon_x^{\max} = W\varepsilon_R = W\frac{\sigma_x^{\text{avg}}}{E_R} \tag{B.7}$$

The shear lag parameter is estimated (Pham 2009, Wu and Pham 2013) by

$$W = 0.7^{S_V / 6D_{\max}} \tag{B.8}$$

where S_V = vertical spacing of reinforcement sheets and $D_{\max}$ = diameter of the largest soil particles.

B.4 Assumption: Sign Convention

By convention, compression is soil is assumed positive by geotechnical engineers, but tension in reinforcement is assumed positive by structural engineers. Thus, the sign in Equation (B.9) is reversed (and the "avg" superscript is discontinued),

$$\varepsilon_x = -W\frac{\sigma_x}{E_R} \tag{B.9}$$

B.5 Hooke's Law

The four assumptions are now combined with Hooke's Law, which is applicable for reinforced soil,

$$\sigma_x - \nu(\sigma_y + \sigma_z) = E_S\varepsilon_x = -W\frac{E_S}{E_R}\sigma_x \tag{B.10}$$

where ν = Poisson's ratio and E_S = Young's modulus for soil. For a pier where $\sigma_x = \sigma_y$, rearrangement gives

$$\frac{\sigma_x}{\sigma_z} = \frac{\nu}{1 - \nu + W\left/\frac{E_S}{E_R}\right.} \tag{B.11}$$

Equation (B.11) has the more useful form,

$$M = \frac{\nu K_P}{1 - \nu + W\left/\frac{E_S}{E_R}\right.} \tag{B.12}$$

where

$$\frac{\sigma_x}{\sigma_z} = \frac{\sigma_H}{\sigma_V} = MK_A \tag{B.13}$$

Poisson's ratio is rarely among data available to the engineer. Fortunately, its effect is secondary to the effects of geometry, reinforcement extensibility, and other parameters.

For an aggregate that drains well, Poisson's ratio can be assumed to be approximately 1/3. This fraction provides the simplification,

$$K / K_A = M = \frac{K_P}{2 + 3W E_S / E_R} \qquad \text{(pier)(B.14)}$$

A similar equation can be derived for walls and abutments in plane strain,

$$K / K_A = M = \frac{K_P}{2 + 2.25W E_S / E_R} \qquad \text{(plane strain)(B.15)}$$

The latter has slightly more mobilization and less deformation.

C. Simplification of Elastic Strain from Hooke's Law

As discussed in Section 2.2.1, the soil component of a reinforced soil composite is assumed to be homogeneous, isotropic, and elastic. Hence, Hooke's law is applicable. It has three equations for normal stresses,

$$\begin{aligned} \varepsilon_x &= \frac{1}{E}\left(\sigma_x - \nu\left[\sigma_y + \sigma_z\right]\right) \\ \varepsilon_y &= \frac{1}{E}\left(\sigma_y - \nu\left[\sigma_z + \sigma_x\right]\right) \\ \varepsilon_z &= \frac{1}{E}\left(\sigma_z - \nu\left[\sigma_x + \sigma_y\right]\right) \end{aligned} \qquad \text{(C.1)}$$

Using K and $E = E_S$ from Appendix D, $\sigma_x = K\sigma_z$. For a square or round pier, $\sigma_y = \sigma_x$, then

$$\begin{aligned} \varepsilon_z &= \frac{1}{E}\left(\sigma_z - \nu\left[\sigma_x + \sigma_y\right]\right) \\ &= \frac{1}{E}\left(\sigma_z - \nu\sigma_x - \nu\sigma_x\right) \\ &= \frac{1}{E}\left(\sigma_z - \nu K\sigma_z - \nu K\sigma_z\right) \\ &= \frac{\sigma_z}{E}\left(1 - 2\nu K\right) \end{aligned} \qquad \text{(C.2)}$$

For a typical wall or abutment, plane strain ($\varepsilon_y = 0$) is assumed, and the second of Equations (C.1) is zero. For plane strain, $\sigma_y = \nu(\sigma_x + \sigma_y)$. Table J summarizes the elastic derivations. Lateral strain is estimated from vertical strain in accord with Section 2.4.

Table J Elastic vertical strain (K and E_S from a quad chart calculation)

	square/round pier	plane strain
vertical strain	$\varepsilon_V = \frac{\sigma_V}{E_S}\left(1 - 2\nu K\right)$	$\varepsilon_V = \frac{\sigma_V}{E_S}\left(1 - \nu K - \nu^2(K+1)\right)$

D. Calculation of K/K_A for Figure 10

The calculation of K/K_A uses the method of Hoffman and Wu (2015). Although values can be calculated for any load, they are calculated here for loads at Points A, B, B', and C, then approximated elsewhere by the method of Section 2.2.3. As in Figure 10, the points are:

- A - at zero load, then $K/K_A = K_P/2$
- B - immediately left of the transition line, determined by Equation (1)
- B' - immediately right of the transition line
- C - at far right, determined by Equation (2)

D.1 System of Three Equations

As in reinforced concrete, Equations (B.14) and (B.15) reveal the importance of the modular ratio, E_S / E_R, for reinforced soil. For reinforcement, E_R is easily determined by Equation (B.3). It involves the extensibility parameter ε_R, which is perhaps the most critical parameter in reinforced soil design.

Young's Modulus for Soil. For soil, E_S is determined by the equation of Janbu (1963) or Lade and Nelson (1987). This paper uses

$$E_S = 100 K_P p_a \left(\frac{\sigma_H}{p_a} \right)^{0.5} \tag{D.1}$$

where σ_H = lateral confining pressure, p_a = atmospheric pressure, and K_P = coefficient for passive lateral earth pressure. Based on data for aggregates (Duncan et al. 1978), the usual coefficient is replaced by $100\,K_P$. It appears illogical to evaluate an elastic constant (E_S) by use of a plastic constant (K_P), but the evaluation is performed on the yield surface where the elastic zone meets the plastic zone.

Lateral Confining Pressure. For Young's modulus, confining pressure σ_H must be estimated. Equation (B.13) is used with Equation (1) for Points B and B'. Equation (B.13) is used with Equation (2) for Point C.

$$\begin{aligned} \sigma_H^{\max} &= MK_A q_{ult} \\ &= MK_A K_P W T_f / S_V \\ &= MWT_f / S_V \end{aligned} \qquad \text{(transition)(D.2)}$$

From $\sigma_H^{\max}$, find the weighted value $w\sigma_H^{\max}$ that provides the average for E_S. This is expected to be approximately $w = 0.5$. Because E_S involves $\sqrt{\sigma_H}$ and the average value of $\sqrt{w}$ for $0 < w < 1$ is 2/3, it follows that $w = (2/3)^2 = 0.44$ and

$$\sigma_H = 0.44 MWT_f / S_V \qquad \text{(transition)(D.3)}$$

For a pier, K/K_A is found by simultaneous solution of Equations (C.1), (C.2), and (B.14). For a wall or abutment in plane strain, use Equation (B.15) instead of (B.14).

D.2 Geosynthetic Calculation. Table K lists parameters for the geosynthetic in Figure 10. At best, they are accurate to two decimal places. So, the calculations of this Appendix keep two digits of accuracy.

Table K. Parameters for Figure 10

T_f reinforcement ultimate strength	4800 lb/ft (70 kN/m)
S_V vertical spacing of reinforcement	8 in (0.2 m)
ε_R reinforcement strain at rupture	10%
ϕ soil's angle of internal friction	45°
D_{max} diameter of largest soil particles	1/2 in (13 mm)

First, the intermediate values are

- $K_P = \tan^2\left(45° + f/2\right) = 5.8$
- $W = 0.7^{S_V/6D_{\max}} = 0.39$ -- Equation (B.8)
- $E_R = \dfrac{T_f}{e_R S_V} = 500$ psi = 0.50 ksi (3.5 MPa) -- Equation (B.3)

Then, the three equations for $M = K/K_A$ at Points A, B, B', and C are

1. $s_H = 0.44MWT_f / S_V = 8.6M$ psi --- at B, B'

   $s_H = 0.44MT_f / S_V = 22M$ psi --- at C

2. $E_S = 100K_P\sqrt{p_a}\sqrt{s_H} = 2200\sqrt{s_H}$ psi $= 2.2\sqrt{s_H}$ ksi --- at B, B', C

3. $M = K_P / 2 = 2.9$ --- at A

   $M = K_P / \left(2 + 2.25W^{E_S/E_R}\right) = 5.8/\left(2 + 1.76E_S\right)$ --- at B

   $M = K_P / \left(2 + 2.25^{E_S/E_R}\right) = 5.8/\left(2 + 4.5E_S\right)$ --- at B', C

At Point A, $K/K_A = 2.9$.

At Point B, the system is solved by the iteration of Table L.

Table L. Iteration at Point B for Figure 10

Equation	iteration 1	iteration 2	iteration 3	iteration 4
$s_H = 8.6M$ psi	2.6	4.3	4.6	4.7
$E_S = 2.2\sqrt{s_H}$ ksi	3.5	4.6	4.7	**4.8**
$M = 5.8/\left(2 + 1.76E_S\right)$	0.71	0.58	0.56	0.56
(M_{init} = 0.3) $M_{average}$:	0.50	0.54	0.55	**0.55**

Two successive values of *M* are averaged. This stabilizes and sometimes accelerates the iteration.

Tables M and N show the iterations for Points B' and C.

Table M. Iteration at Point B', starting from value at Point B

Equation	iteration 1	iteration 2	iteration 3	iteration 4	iteration 5
$\sigma_H = 8.6M$ psi	4.7	3.5	3.0	2.8	2.8
$E_S = 2.2\sqrt{\sigma_H}$ ksi	4.8	4.1	3.8	3.7	3.7
$M = 5.8/(2+4.5E_S)$	0.27	0.28	0.30	0.31	0.31
(M_{init} = 0.55) M_{avg}:	0.41	0.35	0.33	0.32	**0.32**

Table N. Iteration at Point C, starting from value at Point B'

Equation	iteration 1	iteration 2	iteration 3
$\sigma_H = 22M$ psi	7.0	5.8	5.3
$E_S = 2.2\sqrt{\sigma_H}$ ksi	5.8	5.3	5.1
$M = 5.8/(2+4.5E_S)$	0.21	0.22	0.23
(M_{init} = 0.32) $M_{average}$:	0.26	0.24	**0.24**

Observe that average confining pressure σ_H decreases 40% at transition, then it climbs again toward a new maximum. The calculation for steel is similar, but ε_R = 0.0025 is used instead of 0.10.

E. Calculation of K/K_A for TF-7

Table O lists parameters for TF-7 (Nicks et al., 2013)

Table O. Parameters for TF-7

T_f reinforcement ultimate strength	4800 lb/ft (70 kN/m)
S_V vertical spacing of reinforcement	8 in (0.2 m)
ε_R reinforcement strain at rupture	13%
ϕ soil's angle of internal friction	48°
D_{max} diameter of largest soil particles	1 in (0.025 m)
q service load	25 psi (172 kPa)

First, the intermediate values are

- $K_P = \tan^2\left(45° + f/2\right) = 6.8$
- $W = 0.7^{S_V/6D_{\max}} = 0.62$ -- Equation (B.8)
- $E_R = \dfrac{T_f}{e_R S_V} = 385 \text{ psi} = 0.39 \text{ ksi}$ (2.7 MPa) -- Equation (B.3)

Then, the three equations for $M = K/K_A$ at Point B are

1. $s_H = 0.44MWT_f / S_V = 13.6M$ psi --- at B

2. $E_S = 100K_P\sqrt{p_a}\sqrt{s_H} = 2600\sqrt{s_H}$ psi $= 2.6\sqrt{s_H}$ ksi --- at B

3. $M = K_P / \left(2 + 3W^{E_S/E_R}\right) = 6.8 / \left(2 + 4.9E_S\right)$ --- at B

At Point B, the system is solved by the iterations of Table P.

Table P. Iteration at Point B for TF-7

Equation	iteration 1	iteration 2	iteration 3	iteration 4
$\sigma_H = 13.6M$ psi	6.8	4.7	3.9	3.7
$E_S = 2.6\sqrt{\sigma_H}$ ksi	6.8	5.6	5.2	**5.0**
$M = 6.8/(2 + 4.9E_S)$	0.19	0.23	0.25	0.26
(M_{init} = 0.5) $M_{average}$:	0.35	0.29	0.27	**0.26**

The value, K/K_A = 0.26, is highlighted. The final value of E_S (5.0 ksi) is also highlighted because it provides an estimate of elastic strain at transition.

Values at the service load can be found by modifying the first iteration equation by the factor (service load)/(transition load). For TF-7, the factor is 25/185 = 0.135. The first equation becomes σ_H = (0.135)(13.6 M) = 1.8M. Table Q is the iteration at service load.

Table Q. Iteration at service load for TF-7

Equation	iteration 1	iteration 2
$\sigma_H = 1.8M$ psi	0.9	0.88
$E_S = 2.6\sqrt{\sigma_H}$ ksi	2.5	**2.4**
$M = 6.8/(2 + 4.9E_S)$	0.48	0.49
(M_{init} = 0.5) $M_{average}$:	0.49	**0.49**

At service load, K = 0.49K_A = (0.49)(0.15) = 0.074, and E_S = 2.4 ksi.

F. Calculation of K/K_A for GW16

Table R lists parameters for GW16 (Allen and Bathurst, 2003)

Table R. Parameters for GW16

T_f reinforcement ultimate strength	6300 lb/ft (92 kN/m)
S_V vertical spacing of reinforcement	15 in (0.38 m)
ε_R reinforcement strain at rupture	12%
ϕ soil's angle of internal friction	45°
D_{max} diameter of largest soil particles	0.4 in (0.010 m)
q service load	4490 psf (215 kPa)

First, the intermediate values are

- $K_P = \tan^2\left(45° + f/2\right) = 5.8$
- $W = 0.7^{S_V/6D_{\max}} = 0.10$ -- Equation (B.8)
- $E_R = \dfrac{T_f}{e_R S_V} = 290$ psi = 0.29 ksi (2.0 MPa) -- Equation (B.3)

Then, the three equations for $M = K/K_A$ at Point B and B' are

4. $s_H = 0.44MWT_f / S_V = 8.9M$ psi --- at B and B'

5. $E_S = 100K_P\sqrt{p_a}\sqrt{s_H} = 2200\sqrt{s_H}$ psi $= 2.2\sqrt{s_H}$ ksi --- at B and B'

6. $M = K_P / \left(2 + 2.25W^{E_S/E_R}\right) = 5.8/\left(2 + 0.78E_S\right)$ --- at B

$M = K_P / \left(2 + 2.25W^{E_S/E_R}\right) = 5.8/\left(2 + 7.8E_S\right)$ --- at B'

At Point B, the system is solved by the iterations of Table S.

Table S. Iteration at Point B for GW16

Equation	iteration 1	iteration 2	iteration 3	iteration 4
$\sigma_H = 8.9M$ psi	4.5	6.8	7.4	7.6
$E_S = 2.2\sqrt{\sigma_H}$ ksi	4.6	5.7	6.0	6.1
$M = 5.8/(2 + 0.78E_S)$	1.0	0.89	0.86	0.86
(M_{init} = 0.5) $M_{average}$:	0.77	0.83	0.85	**0.86**

The value, K/K_A = 0.86, is highlighted for Point B. Table T iterates for Point B'.

Table T. Iteration at Point B' for GW16

Equation	iteration 1	iteration 2	iteration 3	iteration 4
$\sigma_H = 8.9M$ psi	4.5	2.9	2.3	2.1
$E_S = 2.2\sqrt{\sigma_H}$ ksi	4.6	3.7	3.3	3.2
$M = 5.8/(2 + 7.8E_S)$	0.15	0.19	0.21	0.22
(M_{init} = 0.5) $M_{average}$:	0.33	0.26	0.23	**0.23**

The value, K/K_A = 0.23, is highlighted for Point B'.

G. Calculation of K/K_A for Instrumented GRS Wall

Only Points A and B are needed for the instrumented GRS wall. The service load lies between A and B. Compaction-induced stress (CIS) must be included. Table U lists the parameters.

Table U. Parameters for the instrumented GRS wall

S_V *vertical spacing*	8 in (0.2 m)
CIS, s *compaction stress*	2 psi (14 kPa)
D_{max} *large grain diameter*	0.4 in (10 mm)
ϕ *soil friction angle*	43°
T_f *tensile strength*	4800 lb/ft (70 kN/m)
ε_R *extensibility*	18%

First, the intermediate values are

- $K_P = \tan^2\left(45° + f/2\right) = 5.3$
- $W = 0.7^{S_V/6D_{\max}} = 0.30$ -- Equation (B.8)
- $E_R = \dfrac{T_f}{e_R S_V} = 280$ psi = 0.28 ksi (1.9 MPa) -- Equation (B.3)

Then, the three equations for $M = K/K_A$ at Points A and B are

7. $s_H = 0.44MWT_f / S_V = 6.6M$ psi --- at B

8. $E_S = 100K_P\sqrt{p_a}\sqrt{s_H} = 2000\sqrt{s_H}$ psi $= 2.0\sqrt{s_H}$ ksi --- at B

9. $M = K_P / 2 = 2.65$ --- at A

$M = K_P / \left(2 + 2.25W \frac{E_S}{E_R}\right) = 5.3/\left(2 + 2.4E_S\right)$ --- at B

At Point A, $K/K_A = 2.65$. At Point B, the system is solved by the iterations of Table V.

Table V. Iteration at Point B (no CIS) for GRS Wall

Equation	iteration 1	iteration 2	iteration 3	iteration 4
$\sigma_H = 6.6M$ psi	2.5	2.8	3.1	3.2
$E_S = 2.0\sqrt{\sigma_H}$ ksi	3.1	3.4	3.5	3.6
$M = 5.3/\left(2 + 2.4E_S\right)$	0.55	0.52	0.51	0.50
(M_{init} = 0.3) $M_{average}$:	0.42	0.47	0.49	**0.49**

Then, compaction-induced stress of 2 psi is included in Table W.

Table W. Iteration at Point B for GRS Wall
(CIS = 2 psi is included in the first equation.)

Equation	iteration 1	iteration 2
$\sigma_H = 6.6M$ - 2 psi	1.2	2.0
$E_S = 2.0\sqrt{\sigma_H}$ ksi	2.2	*2.8
$M = 5.3/\left(2 + 2.4E_S\right)$	0.72	0.60
(M_{init} = 0.49) $M_{average}$:	0.61	**0.61**

*due to CIS, $E_S = 2\sqrt{\sigma_H + s} = 2\sqrt{2.0 + 2} = 4.0$ ksi

To obtain accurate values at the service load, the first equation in Table X is modified by the factor (service load / transition load).

Table X. Iteration at service load for GRS Wall

Equation	iteration 1	iteration 2	iteration 3
$\sigma_H = 0.56M$	0.67	0.59	0.54
$E_S = 2.0\sqrt{\sigma_H}$ ksi	1.6	1.5	**1.5**
$M = 5.3/(2 + 2.4E_S)$	0.89	0.93	0.96
(M_{init} = 1.2) $M_{average}$:	1.0	**0.97**	**0.96**

Inclusion of CIS in the first equation gives $\sigma_H = 0.56M - s > 0$. Because the maximum value of M is $K_P / 2 = 2.65$, the maximum CIS is $s = 0.56(2.65) = 1.5$ psi. This gives $E_S = 2.0\sqrt{\sigma_H + s} = 2.0\sqrt{0 + 1.5} = 2.4$ ksi and $K = MK_A = (2.65)(0.19) = 0.50$.

H. Compaction-Induced Stress (CIS) by Broms' Method

Using the analysis of Broms (1974), compaction-induced stress (CIS) is estimated. Broms calculated pressure at a depth by Boussinesq's method, then calculated the lift thickness required to maintain that pressure. The compactor is a Caterpillar model CS-56 on lifts of L = 4 in (10 cm) with ϕ = 43° aggregate. Assume γ = 128 lb/ft^3 (20 kN/m^3).

According to this model's specification, drum width is 7 ft (2.13 m). Its vibratory force ranges upward from 31600 lb (141 kN). With this lower value,

$$\text{line load, } P = \frac{31600}{7} = 4514 \text{ lb/ft} \quad (66 \text{ kN/m}) \tag{H.1}$$

$$\text{maximum CIS, } s_o = 0.8\sqrt{gP} = 608 \text{ psf} = 4.2 \text{ psi} \quad (29 \text{ kPa}) \tag{H.2}$$

$$\text{optimal lift, } L_o = 0.8K_A\sqrt{\frac{P}{g}} = 0.90 \text{ ft} = 10.8 \text{ in} \quad (28 \text{ cm}) \tag{H.3}$$

Because $L < L_o$, the CIS is $s = s_o$ = 4.2 psi (29 KPa). This is consistent with a rule-of-thumb: "CIS of 2 psi (14 kPa) is possible with a walk-behind compactor, and 4 psi (28 kPa) with a large compactor."

The estimated CIS is 4.2 psi for the far zone and 2.0 for the near zone of the instrumented GRS Wall.

I. Wall Section at Instrumentation Line 4 (Shannon & Wilson)

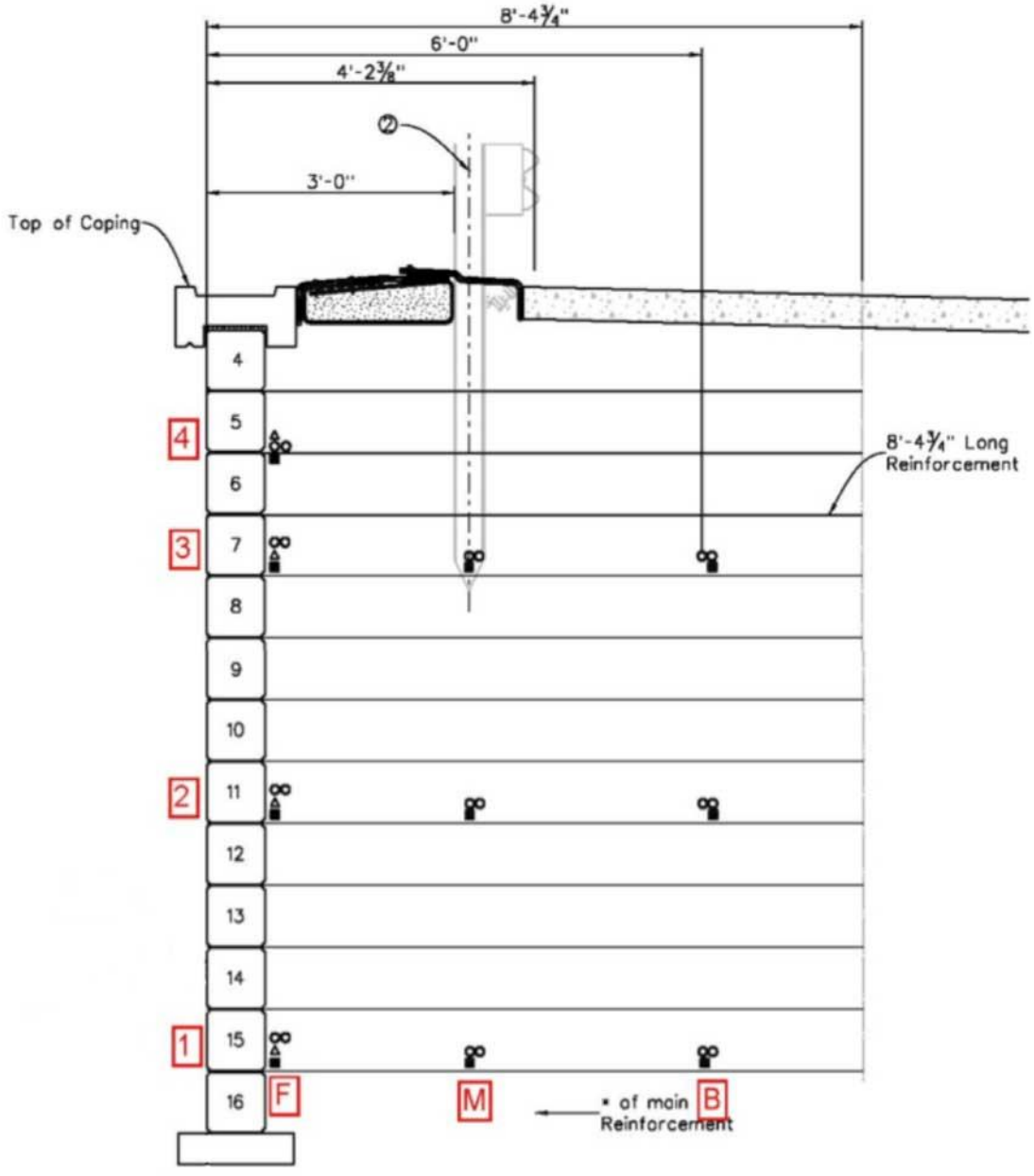

Figure I-1. Section at Instrumentation Line 4 (drawing provided by Shannon and Wilson). As height of the wall must be reduced at various stations, top block courses are removed and instruments at elevation 4 are moved down.

J. Finite Element Analysis (color)

Finite element computations were done with the PLAXIS 8.2 hardening soil model, which requires E_{oed} (the oedometric modulus) as input. The E_{oed} for computation is taken as E_S from Table X, the hand calculation in Appendix G. For lateral deformation, finite element computations and hand calculations agree.

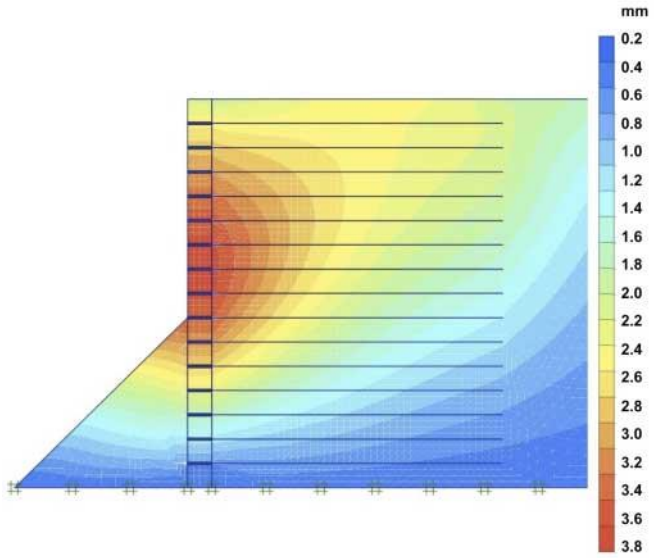

Figure J-1. Horizontal deformation

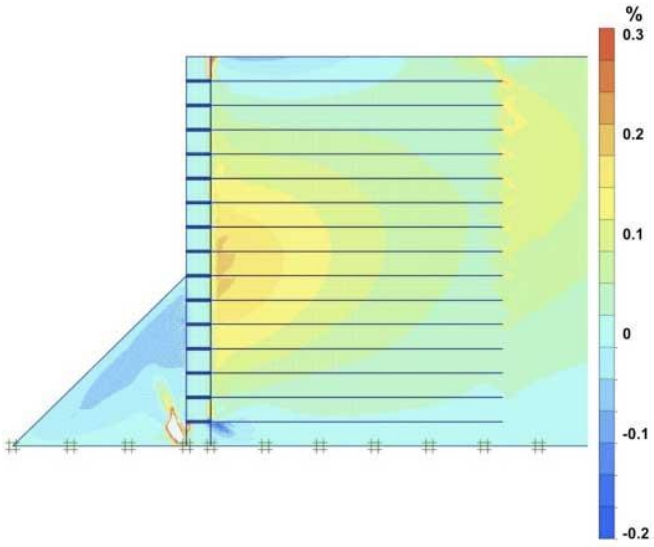

Figure J-2. Horizontal strain

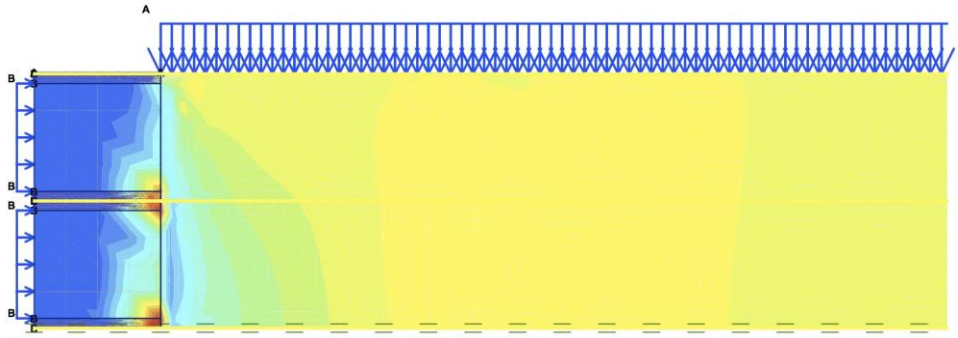

Figure J-3. Friction connection is modeled with sand between blocks to allow slip

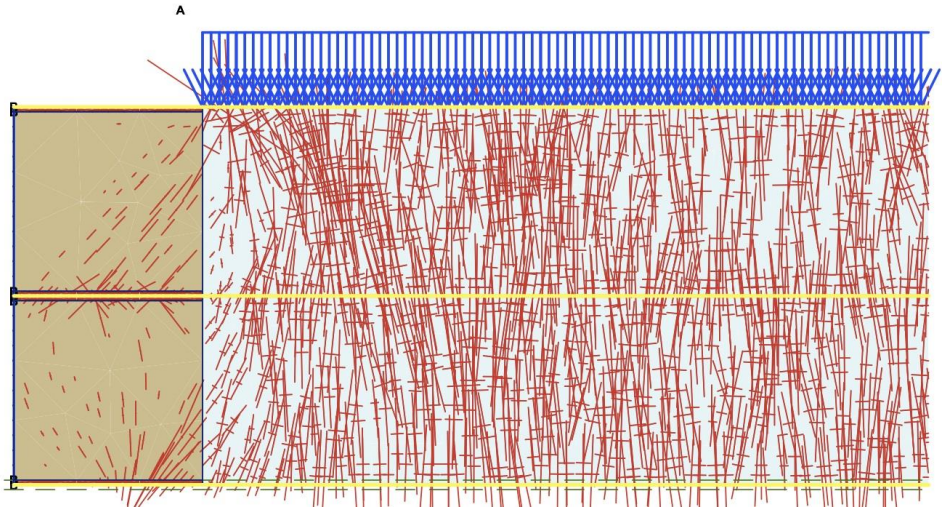

Figure J-4. Stress trajectories flow into facing and enhance friction connection

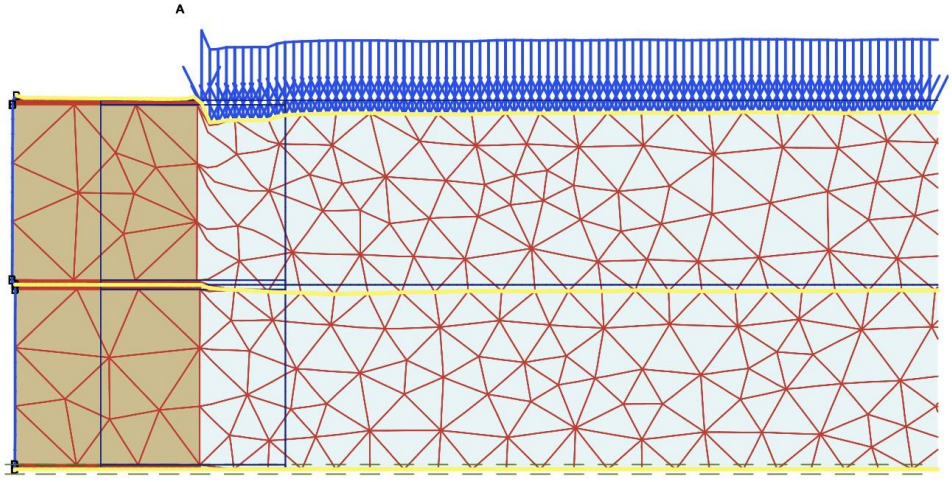

Figure J-5. Vertical strain in the soil causes a scissor effect at the face; therefore, connections must withstand shear as well as tension.

K. Investigation of Secondary Reinforcement (color)

Secondary reinforcement (tails) can be introduced, at a specific service load q, to convert a wall into a GRS wall at the face. Shorter reinforcement provides a final spacing S_V so that $q < q_{ult} = WK_PT_f/S_V$. Reinforcement should not be too short (< 3 feet) as pullout could occur.

The resulting GRS wall, which has secondary reinforcement, is now compared with the GRS wall built entirely of primary reinforcement. The finite element solution of Figure K-1 shows that, using secondary instead of primary reinforcement, lateral deformation at the face increases only 6% relative to Figure I-1. By Equation (9), facing pressure is unchanged because the q_{ult} of the tails-based wall is equal to the q_{ult} of the actual GRS Wall. Of course, this small facing pressure would be hidden by the same compaction-induced stress.

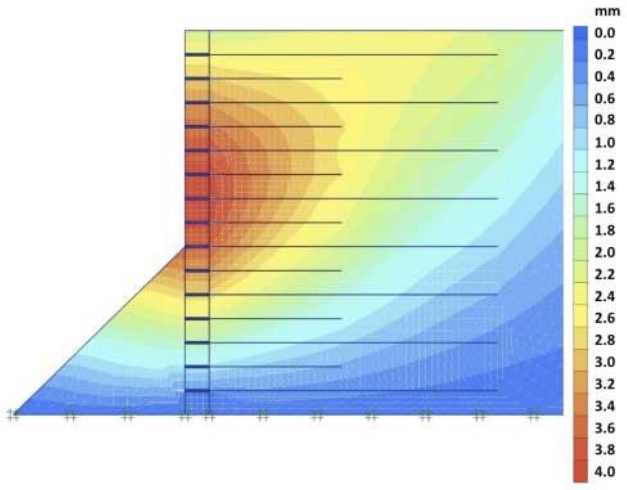

Figure K-1. Lateral deformation using secondary reinforcement

In summary, secondary reinforcement can be used to convert a wall into a GRS wall characterized by low facing pressure. Compared to the equivalent GRS wall built entirely of full-length or primary reinforcement, the penalty is a very slight increase of deformation.

REFERENCES

AASHTO (2012). *LRFD Bridge Design Specifications*. American Association of State Highway and Transportation Officials, Washington, DC.

Adams, M.T., Nicks, J., Stabile, T., Wu, J.T.H., Schlatter, W. and Hartmann, J. (2011). "Geosynthetic Reinforced Soil Integrated Bridge System – Interim Implementation Guide." *Report No. FHWA-HRT-11-026,* Federal Highway Administration, McLean, VA.

Al-Hussaini, M., and Perry, E.B. (1978) "Field experiment of reinforced earth wall." *J. Geotechnical Engineering Division, ASCE*, 104(GT3), pp. 307-322.

Allen, T.M, Christopher, B., Elias, V., and DiMaggio, J. (2001) "Development of the Simplified Method for Internal Stability of Mechanically Stabilized Earth Walls." *Report WA-RD 513.1*, Washington State Department of Transportation, Olympia.

Allen, A.M, and Bathurst, R.J. (2003), "Prediction of Reinforcement Loads in Reinforced Soil Walls," *Report WA-RD 522.2*, Washington State Department of Transportation.

American Institute of Steel Construction [AISC] (2011). *Steel Construction Manual.* Ingram.

Anderson, P.L., Gladstone, R.A., and Sankey, J.E. (2012). "State of the Practice of MSE Wall Design for Highway Structures," *Geotechnical Engineering State of the Art and Practice: Keynote Lectures for GeoCongress 2012*, Oakland, CA.

Bathurst, R.J., Miyata, Y., Nernheim, A., and Allen, A.M. (2008), "Refinement of K-stiffness Method for Geosynthetic-reinforced Soil Walls," *Report HIIFP-095j* ,

Highway Infrastructure Innovation Funding Program, Ontario Ministry of Transportation.

Bathurst, R.J., Nernheim, A., and Allen, T.M. (2009). "Predicted Loads in Steel Reinforced Soil Walls Using the AASHTO Simplified Method," *J. Geotech. Geoenviron. Eng. ASCE* 135, 177-184.

Broms, B. (1974). "Lateral Earth Pressures due to Compaction of Cohesionless Soils," *Proceedings,* 4th Budapest Conference on Soil Mechanics and Foundations Engineering, pp. 373 - 384.

Duncan, J.M., Byrne, P., Wong, K.S., and Mabry, P. (1978). "Strength, Stress-Strain and Bulk Modulus Parameters for Finite Element Analysis of Stresses and Movements in Soil Masses." Report No. UCB/GT/78-02, University of California, Berkeley.

Elmagre, E., and Hoffman, P.F. (2016). "Deformation and Capacity of Vacuum-wrapped Reinforced Soil Test Structures." *Proceedings of the Rocky Mountain Geo-Conference,* 4 Nov 2016, Denver.

Goode, J.C., and Vessely, M.J. (2016). "Installation Summary Report: GRS Instrumentation on I-70 over Smith Road." *Report No. CDOT-2016-06,* Colorado Department of Transportation, Denver.

Hoffman, P.F. (2015). *Plasticity and the Mechanics of Reinforced Soil*. ISBN 1518873391, Preservation Engineering.

Hoffman, P.F. (2016). "Contributions of Janbu and Lade as applied to Reinforced Soil." *Proceedings of the 17th Nordic Geotechnical Meeting,* 25-28 May 2016, Reykjavik.

Hoffman, P.F., and Wu, J.T.H. (2015). "An Analytical Model for Predicting Load-

Deformation Behavior of the FHWA GRS-IBS Performance Test," *International Journal of Geotechnical Engineering*, Vol 9, Issue 2: 150-162.

Iwamoto, M.K., Ooi, P.S.K., Adams and M.T. Nicks, J.E. (2015). "Composite properties from instrumented load tests on mini-piers reinforced with geotextiles." *Geotechnical Testing J.*, American Society of Testing and Materials. 38(4).

Jaky J. (1948). "Pressure in Silos." *Proceedings,* 2nd International Conference of Soil Mechanics and Foundation Engineering, London, Vol. 1, pp 103-107.

Janbu, N. (1963). "Soil Compressibility as Determined by Oedometer and Triaxial Tests," European Conference on Soil Mechanics and Foundation Engineering, Wiesbaden, Germany, Vol. 1, pp. 19-25.

Ketchart, K., and Wu, J.T.H. (1996). "Long-Term Performance Tests of Soil-Geosynthetic Composites" *Report No. CDOT-CTI-96-1*, Colorado Department of Transportation, Denver.

Lade, P.V., and Nelson, R.B. (1987). "Modelling the Elastic Behavior of Granular Materials," *International Journal for Numerical and Analytical Methods in Geomechanics*, 11, 521-542.

Nicks, J.E., Adams, M.T., and Ooi, P.S.K. (2013). "Geosynthetic Reinforced Soil Performance Testing: Axial Load Deformation Relationships," *Report No. FHWA-HRT-13-066*, Federal Highway Administration, McLean, VA.

Terzaghi, K., Peck, R.B., and Mesri, G. (1996). *Soil Mechanics in Engineering Practice*. Wiley.

Timoshenko, S.P., and Goodier, J.N. (1970). *Theory of Elasticity*, McGraw-Hill, New York.

Wu, J.T.H., Lee, K.Z.Z., Helwany, S.B., and Ketchart, K. (2006), "Design and Construction Guidelines for Geosynthetic-Reinforced Soil Bridge Abutments with a Flexible Facing," *NCHRP Report 556*, Transportation Research Board, Washington, DC.

Wu, J.T.H., Pham, T.Q, and Adams, M.T. (2010). "Composite Behavior of Geosynthetic Reinforced Soil Mass." *Report No. FHWA-HRT-10-077*, Federal Highway Administration, McLean, VA.

Wu, J.T.H., and Payeur, J-B. (2014). "Connection Stability Analysis of Segmental Geosynthetic Reinforced Soil (GRS) Walls." *Transportation Infrastructure Geotechnology*, 2(1). DOI 10.1007/s40515-014-0013-4.

Wu, J.T.H. and Pham, T.Q (2013). "Load Carrying Capacity and Required Reinforcement Strength of Closely Spaced Soil-Geosynthetic Composites," *J. Geotech. Geoenviron. Eng. ASCE* 139(9), 1468–1476.

Yang, K-H., Zornberg J.G., and Bathurst R.J. (2010). "Mobilization of Reinforcement Tension within Geosynthetic-Reinforced Structures." *Proceedings of the 2010 Earth Retention Conference*, American Society of Civil Engineers.

Zheng, Y., Fox, P.J, and Shing, P.B. (2015). "Verification of Numerical Model for Static Analysis of Geosynthetic Reinforced Soil Bridge Abutments." Geosynthetics 2015, Portland.